学位論文

Complete loss of ciliary motility in *Ktu*-knockout mice; Insights into tissue-specific mechanisms for rotational polarity

(マウス *Ktu* 変異体を用いた繊毛の配向形成における繊毛の運動性の役割の解析)

平成 24 年 12 月博士（理学）申請

東京大学大学院理学系研究科

生物科学専攻

松尾　萌

Contents

Abbreviations

Ca.: Circa

CCDC: Coiled-coil domain containing

CP complex: Central pair

CSF: Cerebral spinal flow

DAPI: 4',6-diamidino-2-phenylindole

DNAAF: axonemal dynein assembly factor

Hsp: Heat shock protein

IFT: Intra flagellar transport

LRRC: Leucine-rich-repeat

MTEC: Mouse tracheal epithelial cell culture

PCD: Primary ciliary dyskinesia

PCP: Planar cellular polarity

TEM: Transmission electron microscopy

Abstract

Coordinated uni-directional beating is an essential feature of multi cilia in various organs to guarantee proper fluid transport. Recent works have suggested that ciliary motility and planar polarity are required during the process of ciliary alignment to achieve coordinated beating. However, the extent to which ciliary motility is involved in this process in mammals has not yet been fully clarified. Here, in order to address the role of ciliary motility in the process of coordinated ciliary alignment, I analyzed *Kintoun* knockout-mice (*Ktu*$^{-/-}$). *Ktu*$^{-/-}$ exhibited typical phenotypes of PCD with complete loss of ciliary motility in the trachea and brain ependyma. Immunohistochemistry using antibodies against axonemal dyneins confirmed the loss of multiple axonemal dynein components in mutant cilia. Observation of ciliary orientation based on the basal foot direction revealed that ciliary motility was not required for the alignment of airway cilia, whereas a strong requirement was observed in brain ependymal cells. Thus I conclude that the involvement of ciliary motility in the establishment of coordinated ciliary alignment varies among tissues. I propose that the balance of power between fluid flow and planar polarity in establishment of coordinated orientation of motile cilia differ among tissues according to the difference in the stability of the tissue morphology during development.

General introduction

Cilia are hair-like cell organelles that project from the surface of almost all eukaryotic cells and consist of microtubule-based axoneme (9+0 or 9+2 structure) surrounded by a specialized ciliary membrane. The ciliary axoneme is build on the basal body, a derivative of the centriole that is positioned under the cell membrane. This ciliary architecture is highly conserved among species, ranging from protists to mammals. Cilia are generally assembled in differentiated or quiescent cells that exit mitosis (Quarmby and Parker, 2005). Cilia possess receptors for Hedgehog, platelet-derived growth factor (PDGF), Wnt and other signaling molecules on its ciliary membrane. Thus cilia are thought to function as sensors for mechanical and chemical cues from the extra-cellular environment and fine tune the cellular differentiation (Plotnikova et al., 2009). In addition to the above sensory cilia, specialized cilia exist in several organs. Cilia that contain dynein arms are motile and involved in cell motility and extracellular fluid transport (Satir and Christensen, 2007) (Fig. 1B). In mammals, fluid flow driven by motile cilia is important in many organ systems, such as the respiratory tract, the oviduct to the ventricles of the brain. In trachea, hundreds of motile cilia projecting from the apical surface of the epithelial cells beat in the direction from lung to the oral cavity, in order to clear contaminants (mucociliary clearance) (Wanner et al., 1996). Mucociliary clearance plays a pivotal role in the prevention of respiratory disease. Multi ciliated cells lining the walls of ventricles (ependymal cells) generate directed cerebrospinal fluid (CSF) flow that helps CSF homeostasis by transporting secreted guidance factors (Sawamoto, 2006) and nutrients. In addition, this flow guides the long-range migration of neuroblasts along the lateral walls to the olfactory bulb (Sawamoto, 2006). Multi cilia are also important in the process of reproduction, as

sperm requires flagella motility to swim toward the egg and ciliated cells in the female reproductive tract transport eggs from the fallopian tube to uterus. Furthermore in early developmental stages, a leftward flow created by motile cilia in the node determines the left-right body axis. In mice, motile cilia generally grow in a patch–like style, where hundreds of cilia protrude from a single cell. One exception is the node cilia which is solitary (mono cilia). The node cilium is also different in movement, as it shows rotational movement while others move in a waving form. As motile multi cilia is the majority in the mammalian body, we mostly discuss motile multi cilia in this doctoral thesis.

Given its critical and diverse functions, defects in motile cilia in human cause primary ciliary dyskinesia (PCD) which affects one in 16000 people, known as Kartagener syndrome (Fliegauf et al., 2007) (Fig. 1A). Defects in airway cilia cause recurrent respiratory infection such as bronchiectasis and chronic sinusitis. Defective nodal cilia lead to organ mislocation (*situs inversus*), and flagellar and ciliary motility defect in reproductive organs cause infertility (Fliegauf et al., 2007). Stagnation of the CSF flow raises the CSF pressure within the brain ventricles and cause hydrocephalus. In addition, one of the overlooked issues of PCD is that the coordinated uni-direcional alignment of cilia are disturbed in some of the PCD patients (Rautiainen et al., 1990). Thus, it is assumed that ciliary disorientation is a byproduct of abnormal ciliary motility.

In previous reports, a question as to how PCD occurs by motile ciliary defects has been addressed using various knockout mice, including ciliary motility defect mutants. However, they have several problems. First, cilia retained residual motility in most of ciliary mutants used. Indeed, previous reports mentioned that weakend beating of mutant cilia is sufficient to disrupt the overall flow and they did not precisely assess the

effect of the residual motility. As is suggested in recent papers, the role of ciliary motility is not only production of the extra-cellular flow but also enhancement of the ciliary sensory function (Mitchell et al., 2007). Thus defective beating could have some roles. Furthermore, some of the studies used knockout mice with ciliogenesis defects in addition to motility defects, which made the analyses complicated. Finally, as described above, ciliary disorientation was interpreted as a result of ciliary motility defects in PCD patients. In general, ciliary motility was simply regarded as a flow generator and was thought to have less effect on ciliary development. However recent reports suggested that ciliary motility may play a role in ciliary development (alignment). However, previous studies of mice mutants with ciliary motility defects did not examined this possibility. Taking all these problems into account, a knockout mouse that shows complete loss of ciliary motility in multiple organs is required to understand the role of ciliary motility in development more precisely.

For this purpose, I focused on a cytoplasmic protein Kintoun (Ktu) in this thesis. In the *ktu/pf13* medaka mutant, outer and a part of inner dynein arms are missing, leading to a complete loss of motility. As Ktu is required for axonemal dynein pre-assembly, depletion of Ktu was expected to disrupt the assembly of multiple dyneins, leading to greater reduction of ciliary motility than previously reported for mouse models (Fig. 1C). Thus I generated and analyzed *Ktu*-knockout mice ($Ktu^{-/-}$). In the present thesis, I first characterized murine Ktu *in vivo* and *in vitro* using immunohistochemistry (chapter 1). In the second chapter, detailed phenotypic analysis of $Ktu^{-/-}$ mice was performed. As expected, the mutant mice exhibited a complete loss of ciliary motility in trachea and brain ventricles, providing an ideal model of PCD (chapter 2). In the last chapter, using $Ktu^{-/-}$ mice, I examined the requirement of ciliary motility in the establishment of the

rotational polarity of the cilium/basal body in brain ependyma and trachea epithelia. My results demonstrate that ciliary motility is required for the unidirectional alignment of cilia in the brain ependyma, but not in the tracheal ciliated cells (chapter 3). Thus I conclude that the involvement of ciliary motility in their orientation differs dramatically among organs.

Chapter 1: Characteristics of mouse Kintoun (Ktu)

Introduction

Motile cilia develop specifically in cells that express specific transcription factors that regulate ciliogenesis such as Foxj1 and Rfx3 (Thomas et al., 2010). In general, ciliogenesis begins with the generation of a basal structure called “basal body”. Unlike a cell producing solitary cilia (mono cilia) in which a single basal body is generated only from the duplication of mother centrioles, massive numbers of additional basal bodies are produced from non-microtubule-based structure called “deuterosome” in the cytoplasm of a multi-ciliated cell (Dirksen, 1991; Hagiwara et al., 2004). Basal bodies dock to the cell surface and protrude cilia. Intraflagellar transport (IFT) proteins transport ciliary proteins (membrane components, receptors, dynein components, accessory proteins and so on) between the cytoplasm and ciliary compartments. As cilia lack translational machineries, ciliary components are produced in the cytoplasm and transported to cilia via IFT.

Ciliary motility is generated by two types of axonemal dyneins, inner arm dynein and outer arm dynein. Axonemal dyneins are protein complexes that consist of three types of proteins, light chains, intermediate chains and heavy chains (Fig. 1B). The core ciliary components for motility (the central pair complex, the radial spoke) are also important for proper beating of cilia. Like other ciliary proteins, axonemal dynein components are produced in the cytoplasm and transported to cilia during ciliogenesis. It was reported that the axonemal dynein complex is assembled in the cytoplasm and transported to the ciliary compartment (Fowkes and Mitchell, 1998). Thus, proteins that are involved in dynein assembly are also essential for ciliary motility. Today, several cytoplasmic proteins in these groups have been identified including Leucine-rich-repeat (LRR) containing protein LRRC50 (Duquesnoy et al., 2009; Loges et al., 2009),

DNAAF3 (Mitchison et al., 2012). Kintoun (Ktu) is one of the earliest known proteins that function in cytoplasmic dynein pre- assembly (Omran et al., 2008).

The *ktu* gene was first identified in a medaka mutant showing a defect in left-right patterning, and found to be the causative gene for some PCD human patients and the *pf13* mutant of *Chlamydomonas*. Subsequent genetic and biochemical analyses revealed that Ktu is required for preassembly of axonemal dyneins in the cytoplasm (Omran et al., 2008). Further analysis showed the interaction of Ktu with dynein intermediate chain DNAI2 and heatshock protein Hsp70. Thus Ktu is thought to form a pre-assemble dynein complex in the cytoplasm with Hsp70 (Fig. 1C). The previous study explored the function of Ktu in medaka, mouse, human and *Chlamydomonas* (Omran et al., 2008), but the expression of Ktu in tissues and cells was not examined in detail except for in the medaka renal tubule. To analyze whether the expression of Ktu is similar in mammals as in fish, I first examined the characteristics of murine Ktu.

Materials and Methods

Section immunohistochemistry (IHC)

Mice were killed and tissues were isolated in ice-cold PBS. Tissues were mounted in Tissue-Tek O.C.T. compound (Sakura finetek) and frozen in liquid nitrogen. Frozen samples were sectioned by cryostat into 12-16 μm thick sections (12 μm for trachea, 16 μm for brain). Sections were dried and fixed with 4% PFA/PBS for 10 min and permeabilized with 0.5% or 10% triton X-100 for 10 min. When staining with anti-Tuj1 or anti-S100β brain samples were dissected and fixed in 4% PFA overnight at 4ºC. After cryoprotection by 20% sucrose/PBS, brains were mounted in O.C.T. compound and sectioned as described above. After washing sections with PBS or PBDT, sections were blocked with 5% BSA or 5% skim milk diluted in PBS. Primary antibodies were diluted in PBS or 1% skim milk and incubated for 2 h at room temperature (or overnight at 4ºC). After incubation, sections were washed in PBS or PBDT for 10 min, three times. Secondary antibodies were diluted in PBS or 1% skim milk and incubated for 2 h at room temperature and washed by PBS or PBDT for 10 min, three times. For some samples, double or triple staining with DAPI or rhodamine phalloidin (Invitrogen, R415) was performed. Sections were mounted with 50% glycerol and analyzed by confocal microscopy (LSM 710, Zeiss). Primary antibodies used in IHC are as follows: Mouse anti-Foxj1 mAb (1:250; eBioscience, 14-9965-80), mouse anti-acetylated α-tubulin mAb (1:500; Sigma, T7451), mouse anti-S100β mAb (1:300; Sigma, S2532), mouse anti-TUJ1 mAb (1:300; Covance, MMS-435P), rabbit anti-Ktu pAb (1:200; Omran et al., 2008). Secondary antibodies are donkey anti-mouse Alexa 488/555/647 (Invitrogen), donkey anti-rabbit Alexa 488/555 (Invitrogen), donkey anti-goat Alexa 647 (Invitrogen). Secondary antibodies were used with a dilution of 1:250.

Western Blotting

Tissues were dissected in ice-cold PBS and homogenized in HMEK buffer containing NP-40 (10 mM HEPES, 5 mM $MgSO_4$, 5 mM EDTA, 25 mM KCl, complete protease inhibitor cocktail (Roche), 0.25% NP-40) as protein samples. Protein samples were boiled with 2x SDS buffer (0.1 M Tris-HCl (pH 6.8), 20% Glycerol, 4% SDS, 10% 2-mercaptoethanol, 0.01% BPB) and separated by 5%, 7%, 10% polyacrylamide gels. Gels were transferred onto PVDF membranes (Millipore) and blocked with 5% skim milk/PBS (Morinaga) for 1h at room temperature. Primary antibodies were diluted in PBS or 1% skim milk and incubated for 2 h at room temperature or overnight at 4ºC. After serial washing with PBST, membranes were incubated with secondary antibodies. Protein bands were visualized using ECL prime kit (GE) or Chemilumi one kit (Funakoshi) and detected by ImageQuant (GE Healthware).

Antibodies used in western blotting are as follows: rabbit anti-Ktu pAb (1:1500) (Omran et al., 2008), goat anti-actin pAb (1:3000; Santa Cruz, sc-1616), anti-rabbit HRP (1:3000; Sigma, A0545), anti-goat HRP (1:3000; Chemicon, AP106P).

In vitro mouse trachea epithelial cell culture (MTEC)

MTEC was produced using methods described previously (You et al., 2002). For MTEC production, mice, 3-5 week of age were used. After cervical dislocation, mice were briefly soaked to 70% ethanol. Trachea (from larynx to near bronchial main branches) was dissected from the surrounding tissues. Trachea was trimmed of excess muscle and connective tissues in ice-cold Ham's F-12 (Ham's F-12 containing 100 U/ml penicillin, 100 μg/ml streptomycin, 10 mM HEPES pH7.4). Tracheal epithelial cells

were collected by pronase digestion (Ham's F-12 containing 1.5 mg/ml pronase) at 4ºC overnight (16-18 h). In general, 200 μl/ trachea of pronase solution was used. Samples were gently shaked several times during the incubation. Sample tubes were put on ice and FBS was added (final 10%). Sample tubes were inverted for 12 times and tracheas were transferred to another tube with Ham's F-12 with 10% FBS and inverted. Tracheas were transferred to another tube with Ham's F-12 with 10% FBS and inverted to further release cells. The collected cells were centrifuged at 400 G for 10 min at 4ºC. Supernatants were discarded and cell pellets were resuspended in Ham's F-12 containting DnaseI (Ham's F-12 containing 100 U/ml penicillin, 100 μg/ml streptomycin, 10 mM HEPES pH7.4, 0.5 mg/ml pancreatic DnaseI, 10 mg/ml BSA). Samples were incubated on ice for 5 min. After centrifugation (400 G for 5 min at 4ºC), cell pellets were resuspended in MTEC basic media FBS (DMEM-Ham's F-12 (1:1 vol/vol), 15 mM HEPES, 100 U/ml penicillin, 100 μg/ml streptomycin, 0.25 μg/ml fungizone) with 10% FBS and incubated in tissue culture dish for 3-4 h in 5% CO_2 at 37ºC to eliminate fibroblasts. After incubation, non-adherent cells in the medium were collected by centrifugation (400 G for 5 min at 4ºC) and resuspended to MTEC/PLUS (MTEC basic media supplemented with 10 μg/ml insulin, 5 μg/ml transferrin, 0.1 μg/ml cholera toxin, 25 ng/ml epidermal growth factor, 30 μg/ml bovine pituitary extract, 5% FBS, 0.01 μM retinoic acid) seeded on polyester membrane dishes (Transwell). Polyester membrane dishes were coated by 50 μg/ml type I rat tail collagen diluted in 0.02 N acetic acid. Cells were cultured in 5% CO_2 at 37ºC to reach confluent. Media filling upper and lower chambers were changed every 2 days. 2 days after confluent, media in the upper chamber was removed to establish air-liquid interface (ALI), while the media in the lower chamber was changed to a MTEC/NS (MTEC basic

supplemented with 2% NuSerum (BD) and freshly added 0.01 μM retinoic acid). After several days of incubation, cultured cells were fixed with 0.5% PFA/PBS for 5 min followed by –20ºC MetOH for 7 min. Cells were permeabilized with 0.5% Triton-X 100 for 3 min. Samples were blocked wih 5% BSA for 30 min and incubated in primary antibodies for 2 h at room temperature. After incubation, samples were washed with PBS (10 min x3) and incubated with secondary antibodies for 30 min. Samples were washed and mounted with 50% glycerol/PBS between slide glass and coverslip. Dilution of primary and secondary antibodies was the same as the protocol for section IHC.

Results

Ktu is expressed in multiciliated tissues.

I started the analysis of murine Ktu with western blots to various tissues from P14 mice using a specific antibody to murine Ktu. Ktu protein was detected as a band around 120 kDa as previously reported (Omran et al., 2008). In mouse, Ktu is expressed in all tissue that harbor motile cilia or flagella, high in testis and moderate to low in oviduct, trachea and brain. In contrast, Ktu expression was undetectable in other non-ciliated organs such as spleen and heart (Fig. 2A). We then examined the subcellular localization of Ktu in multiciliated mouse tissues by immunohistochemistry. Tracheal tissues taken from new born mice at P14 were immunolabeled with anti-Ktu, acetylated α-tubulin (a marker for cilia), IFT88 (a component of the intraflagellar transport machinery present in cilia) and Foxj1 antibodies. Foxj1 transcription factor is a master regulator of the motile ciliogenic program (Yu et al., 2008) and exclusively expressed in cells that develop motile cilia (Blatt et al., 1999; Hackett, 1995; Jacquet et al., 2009). Thus Foxj1 demarcates ciliated cells in the tracheal epithelium that consists of multiciliated cells and non-ciliated cells including goblet cells. In the tracheal epithelium, Ktu is expressed only in Foxj1-positive cells and is present broadly in the cytoplasm (Fig. 2C). There was no signal detected in the ciliary compartment (Fig. 2B).

The walls of the lateral ventricles of the brain at P7 are mostly lined by ependymal cells as shown by the localization of S100β (calcium binding protein, a marker for ependymal cells) (Jacquet et al., 2009) (Fig. 2E), whereas neurons positive for Tuj1 (Neuronal class III beta-tubulin) are present underneath the ependymal layer (Fig. 2F). In lateral ventricles, Ktu is exclusively detected in ependymal cells and again, its subcellular localization is broad except for in nuclei (Fig. 2D-F). In the medaka renal

epithelium, however, Ktu was reported to be localized in the apical portion of the cells (Omran et al., 2008). This apparent discrepancy in subcellular localization between mouse and fish could be due to the timing of observation; as the observation was performed against adult tissues with mature cilia in the medaka kidney whereas the observation in mice may have been done in much earlier stages. Ktu may change distribution depending on the step of ciliogenesis.

Ktu expression in cultured tracheal cells

To monitor Ktu distribution at all steps of ciliogenesis, I applied mouse tracheal epithelial cell (MTEC) culture system, which is known to faithfully model ciliogenesis in the tracheal epithelium *in vivo* (You et al., 2002) (Fig. 3A). The culture is started by seeding tracheal cells isolated from P21-35 mice onto a porous filter suspended in medium. During plating, most ciliated cells are unable to attach to the filter so that ciliogenesis will start *de novo* in this system. Under submerged conditions, cells proliferate into a confluent state that resembles a polarized epithelium. Ciliogenesis is then induced by placing cells in an air–liquid interface. A certain proportion of cells begin ciliogenesis 2 - 3 days after induction and differentiate into a maximally ciliated epithelium at ~14 days (fig. 3B). Similar to *in vivo* situations, Ktu is expressed exclusively in Foxj1-positive cells in MTECs (Fig. 3C). Ciliogenesis did not proceed synchronously among ciliated cells in vitro under our experimental conditions. Some cells (ca.10%) began to express Ktu in the cytoplasm 2 days after induction. Ktu is broadly and evenly distributed throughout the cytoplasm, at time points at which cilia are not yet visible on the cell surface (Fig. 4A, B). I noticed that a few cells express Foxj1 but not Ktu (asterisk in Fig. 3C), suggesting that Ktu can be placeddownstream of

Foxj1. At subsequent stages, localization of Ktu did not change significantly (Fig. 4A, B). Axonemal dynein heavy chain DNAH5 was already localized to young short cilia (Fig. 4C) in cells at the early ciliogenesis stage (as shown in cell 2 in Fig. 4B), suggesting that Ktu becomes functional in the cytoplasm to assemble axonemal dyneins before cells start morphological ciliogenesis.

Discussion

We have investigated the expression and subcellular localization of murine Ktu using the specific antibody. In adult mice, Ktu is highly to moderately expressed in organs that develop motile cilia/flagella, and in these organs only ciliated cells express Ktu (Fig. 2A). Broad and uniform distribution of Ktu was frequently observed in the cytoplasm of differentiated ciliated cells (Fig. 2B). An *in vitro* culture system (MTEC) further demonstrated that tracheal cells start to express Ktu just before the onset of ciliogenesis and maintain expression until cilia are fully developed (Fig. 4A, B). Upon induction in MTECs, a certain proportion of tracheal cells develop multi-cilia *de novo* and Foxj1 is expected to regulate the process of ciliogenesis as a master regulator (You et al., 2004). Ktu is likely to function downstream of Foxj1 because at an early step of differentiation, some cells express only Foxj1 but not Ktu, while Ktu is expressed exclusively in Foxj1-positive cells (Fig. 3C). MTEC also demonstrates that subcellular localization of Ktu does not significantly change during the entire process of ciliogenesis. This observation appears to conflict with our previous finding in the medaka renal epithelium in which Ktu mainly localizes to the apical cytoplasm (Omran et al., 2008). This may reflect a difference in cell type; medaka renal cells have a single motile cilium, while tracheal cells generate and maintain hundreds of cilia during differentiation and growth, requiring a large amount of ciliary components including axonemal dyneins. In conclusion, murine Ktu expresses exclusively in motile ciliated cells which is consistent with previous report suggesting a conserved function of Ktu in dynein pre-assembly in cytoplasm.

Chapter 2: Phenotypic analysis of *Ktu*-knockout mice

Introduction

Ciliary motility is controlled by the coordinated interaction between microtubule doublets and axonemal dyneins. The axonemal dynein on A-tubules produce ciliary motility through ATP-dependent sliding on neighbouring B-microtubules. The radial spoke and the central pairs are involved in beat regulation. Coordinated activation/inactivation of inner and outer arm dynein arms generate beating of cilia (Salathe, 2007). Inner-arm dynein is responsible for the bending form of the cilia. On the other hand, outer-arm dynein regulate the beat frequency (Chilvers et al., 2003; de Iongh and Rutland, 1995). Mutations of these dyneins greatly affect the ciliary motility and/or beat frequency. Indeed reduction of ciliary motility was observed in PCD patients lacking axonemal dynein components such as DNAI1, DNAI2, DNAH5 (IC1, IC2, γ-HC respectively in *Chlamydomonas*) (Loges et al., 2008; Olbrich et al., 2002; Pennarun et al., 1999). However, due to the complementary functions among components, knockout mice with a deletion in any of dynein components were reported to possess residual ciliary motility. For example, the knockout mouse of DNAH5, a component of outer arm dynein heavy chain retained residual motility in brain ependyma (Ibanez-Tallon, 2004). To make matters complicated, tissue-specific phenotype was observed, as complete loss of motility in the trachea. As Ktu is required for dynein complex formation, we expected that *Ktu*-knockout mice would exhibit severe ciliary motility defect than any dynein mutant mice. Thus I expected that $Ktu^{-/-}$ would provide an ideal model that exhibit complete loss of ciliary motility in multiple organs.

Here, I show that $Ktu^{-/-}$ exhibits typical phenotypes of PCD. Cilia of $Ktu^{-/-}$ were completely immotile in brain ependyma and trachea epithelial cells. Subsequent

analysis showed reduction in expression of axonemal dynein components. Thus I conclude that *Ktu*$^{-/-}$ is a novel PCD model suitable for the investigation of motific-specific phenotypes such as ciliary orientation.

Material and Methods

Generation of knock-out mouse

I generated a targeting vector with a floxed neo cassette to replace the 1st exon of *Ktu*, which would thus remove a translational initiation codon to produce a null allele. The linearized vector (25 μg) was electroporated into TT2 ES cells (Yagi et al., 1993). G418-resistant cell clones were further selected by PCR. Correct homologous recombination was confirmed by Southern blotting analysis and targeted cell clones were aggregated with MCH (a closed ICR colony established at CLEA Japan Inc., Tokyo, Japan) 8-cells and transferred to pseudopregnant female recipients. The resulting chimeric mice were bred with MCH females. Germline transmission of the targeted allele was confirmed by PCR. The floxed neomycin cassette was later removed by breeding with a CAG-Cre transgenic mouse (Sakai and Miyazaki, 1997). The established $Ktu^{+/-}$ line was intercossed to produce homozygous $Ktu^{-/-}$ mice (Fig. 5A). Genotype of the mice was determined by PCR polymorphism. Amplification by primer set of 1 and 2 (1&2) generate DNA fragment of 600bp, whereas amplification by primer set of 1 and 3 (1&3) generate DNA fragment of 300bp. (primer1: 5'-GGAGACATCTGATGGACAGTTGATG-3', primer2: 5'-TACCACTGAGCCA CACACCCAGG-3', primer3: 5'-GGC AGCGAGAGCCGCAGCCGGTAGTC-3'). $Ktu^{+/+}$: 1&2 (+) 1&3 (-), $Ktu^{+/-}$: 1&2 (+) 1&3 (+), $Ktu^{-/-}$: 1&2 (-) 1&3 (+). $Ktu^{-/-}$ were also identified visually by enlarged head and abnormal location of milk spot. All experiments were performed with the approval of the animal experiment ethics committee at the University of Tokyo according to the University of Tokyo guidelines for the care and use of laboratory animals.

Histology

Mice were killed and tissues were dissected in ice-cold PBS. Brains were fixed in 4% PFA/PBS overnight at 4ºC. After cryoprotection by 20% sucrose/PBS, brains were mounted in Tissue-Tek O.C.T. compound (Sakura finetek) and sectioned into 20 μm slices in -20 ºC. Sections were immersed in 70% Ethanol for 4 h and dehydrated. They were then rinsed with water and stained with hematoxylin and eosin. After being substituted with Clear plus (Farma), sections were mounted with Entellan new (Merck).

Production of antibody

Rabbit polyclonal antibodies against mouse DNAH5 and DNAH9 were produced as follows. To produce antigen, mDNAH5 cDNA fragment (nt 2752-3621 of NM_133365) and mDNAH9 cDNA fragment (nt 3094-4143 of NM_001099633) was obtained by PCR using set of primers (DNAH5, primer 1&2; DNAH9, primer 3&4) and subcloned into pET24a plasmid. His-tag fused protein was produced in *Escherichia coli* strain, BL21. The fusion protein was purified with Ni-NTA agarose beads (Millipore) and immunized to rabbits for polyclonal antibody production. Antiserum was purified with CNBr-Sepharose beads (GE) and used for western blotting and immunohistochemistry. The primer sequences are in the followings (underlined letters represent restriction enzyme sites). Primer1: GTCGACAAGACCCCCTGACTTGTGA AGAA, Primer2: GCGGCCGCGTCCATGGATGTGATAACTTC, Primer3: GTCGAC AATATAGAA GAAATACCCTCAGCCAG, Primer4: GCGGCCGCTGCATCCCAGGACCTGAAC TC. The amino acid sequences for the antigen are as follows.

AnARKK

Section immunohistochemistry (IHC)

Mice were killed and tissues were isolated in ice-cold PBS. Tissues were mounted in Tissue-Tek O.C.T. compound (Sakura finetek) and frozen in liquid nitrogen. Frozen samples were sectioned by cryostat into 12-16 μm thick sections (12 μm for trachea, 16 μm for brain). Sections were dried and fixed with 4% PFA/PBS for 10 min and permeabilized with 0.5% or 10% triton X-100 for 10 min. After washing sections with PBS or PBDT, sections were blocked with 5% BSA or 5% skim milk diluted in PBS. Primary antibodies were diluted in PBS or 1% skim milk and incubated for 2 h at room temperature (or overnight at 4ºC). After incubation, sections were washed in PBS or PBDT for 10 min, three times. Secondary antibodies were diluted in PBS or 1% skim milk and incubated for 2 h at room temperature and washed by PBS or PBDT for 10 min, three times. For some samples, double or triple staining with DAPI or rhodamine phalloidin (Invitrogen, R415) was performed. Sections were mounted with 50% glycerol and analyzed by confocal microscopy (LSM 710, Zeiss). Primary antibodies used in IHC are as follows: mouse anti-DNAI2 mAb (1:250; Zymed), rabbit anti-DNAI1 pAb (1:250; Sigma, HPA021649), mouse anti-acetylated α-tubulin mAb (1:500; Sigma, T7451), rabbit anti-α-tubulin pAb (1:300, Abcam), goat anti-IFT88 pAb (1:300; Everest, EB07088). Secondary antibodies are donkey anti-mouse Alexa 488/555/647 (Invitrogen), donkey anti-rabbit Alexa 488/555 (Invitrogen), donkey anti-goat Alexa 647. Secondary antibodies were used with a dilution of 1:250.

Video microscopy of cilia motility

Animals were killed and trachea and brain were isolated in PBS. Trachea were opened longitudinally and lateral ventricles were dissected from brain ventricles.

Tissues were sectioned into thin strips using a microsurgery knife (MANI) (~0.5 mm). Sections were placed on slide glasses with holed electrical tape and mounted with pre-warmed sHBSS (HBSS+25 mM Hepes). Beating cilia were captured at 26 frames per second by ARTCAM 130MI-BW (Artray) camera connected to BX61 (Olympus) microscope.

Results

Generation of Ktu$^{-/-}$

Since *ktu/pf13* mutation results in complete loss of ciliary motility in *Chlamydomonas* and medaka Kuppfer's vesicle, an organ equivalent to the mouse node, I expected the same phenotype in *Ktu*$^{-/-}$ mice, which allowed us to examine the direct relationship between ciliary motility and orientation. I thus generated *Ktu*$^{-/-}$ mice, in which exon1 had been deleted through a Cre-recombinase based technique (Fig. 5A). Mice were genotyped using specific primers (Fig. 5B). A western blot analysis showed the absence of Ktu protein at 120kDa in Ktu-deficient mice (Fig. 5C). Furthermore, cytoplasmic localization of Ktu was lost in trachea epithelial cells (Fig. 5D). These results confirmed that no functional Ktu is produced from the mutated allele.

Ktu-knockout mice exhibit primary ciliary dyskinesia.

Following normal Mendelian inheritance, approximately 25% of the pups born from *Ktu*$^{+/-}$ intercrosses were homozygous *Ktu*$^{-/-}$ mutants. Some of the *Ktu*$^{-/-}$ mice died during the initial 1-2 days after birth. Most of the pups that survived the neonatal period showed a reduced rate of weight gain, resulting in small body size (Fig. 6A). More than 90% of the *Ktu*$^{-/-}$ mice died before weaning. Translocation of circular (heart) and abdominal organs (stomach and spleen) was frequently reversed in *Ktu*$^{-/-}$ pups (17 out of 43). This randomized positioning is a typical phenotype of PCD and referred to as *situs inversus totalis* (Fig. 6B). The ratio of *situs inversus* occurrences was 40% in *Ktu*$^{-/-}$ (n= 43) (Fig. 6C). *Ktu*$^{-/-}$ also exhibited another typical phenotype of PCD, hydrocephalus (Fig. 6D-F). Coronal sections of P14 brains of *Ktu*$^{-/-}$ showed enlarged fluid-filled brain ventricles which represents hydrocephalus (Fig. 6F, yellow arrow). Enlargement of the

lateral ventricles were accompanied by thinning and rarefaction of the cerebral cortex.Due to the accumulation of CSF, cerebrum is enlarged and the olfactory bulb and cerebellums is compressed (Fig. 6E). We further examined the development of hydrocephalus by making serial sections of mutant brains of different stages. At embryonic day 18.5 (E18.5), brains from *Ktu*$^{-/-}$ mice were indistinguishable from those of controls (heterozygous and wild-type littermates) and did not show any indication of hydrocephalus (data not shown). At P0.5, lateral ventricles of the *Ktu*$^{-/-}$ started to enlarge and gradually became enlarged during the course of development (N=6/6) (Fig. 7). Hydrocephalus was not observed in human *KTU/pf13* patients (Omran et al., 2008). This may be due to the difference in the size of ventricles suggesting that narrower canals are sensitive to CSF flow retardation caused by ciliary motility defect. Although renal cysts were observed in medaka *ktu*, the overall morphology of *Ktu*$^{-/-}$ kidneys were normal and devoid of cysts. In general, fish kidneys possess motile cilia whereas mouse kidneys are devoid of motile cilia. We suspect that this morphological difference is the cause of this difference in phenotypes.

As described above, the survival rate of homozygous mutants decreased as embryonic and postnatal development proceeded, and most mutants died by around stage P21. This poor viability of *Ktu*$^{-/-}$ mice prevented investigation of later developing organs such as the oviduct, one of the well-studied ciliated tissues. I thus focused on the tracheal epithelium and ventricles of the brain in the following experiments.

As components of the axonemal dynein were reduced in patients with *KTU* mutation, I investigated the expression and distribution of axonemal dyneins in *Ktu*$^{-/-}$ mutant cells by immunohistochemistry. In brain ependymal cells of P7 mice, outer arm dynein heavy chain DNAH5, DNAH9 and intermediate chain DNAI1 and DNAI2, all localized to

cilia in *Ktu*$^{+/+}$ (Fig. 8). However, positive signals were completely lost in mutant cilia (Fig. 8). The same was true for tracheal epithelial cellsexcept for DNAH9 (Fig. 9A, C, D). In trachea epithelial cells, there was a residual signal of DNAH9 in the ciliary tip (Fig. 9B). These results suggest that incorporation of axonemal dynein components to cilia is severely affected in *Ktu*$^{-/-}$ mice. The loss of DNAH9 from ciliary axoneme is consistent with the result of trachea epitheilial cells of human *KTU/pf13* patients (Omran et al., 2008). However DNAH5 and DNAI2 is lost from the distal tip of cilia but retain its localization in the proximal axonemes in human patients (Omran et al., 2008). This difference may be due to the difference in the requirement of Ktu for dynein pre-assembly among species.

To further confirm the above results, I performed transmission electron microscopy (TEM). TEM analysis revealed that both outer and inner dynein arms attached to the doublet of microtubules were lost in *Ktu*$^{-/-}$ cilia of tracheal epithelial cells (Fig. 9E) and ependymal cells (not shown). Finally, I examined the motility of cilia in *Ktu*$^{-/-}$ mice at P7 by video microscopy. In wild-type mice, multi cilia of both trachea epithelial cells and brain ependymal cells beat vigorously, but mutant cilia were paralyzed and completely lost their motility. Taken together, *Ktu*$^{-/-}$ mice completely lack cilia motility due to failure in dynein arm formation, despite normal ciliogenesis, thus providing an ideal PCD model to assess rotational polarity.

Discussion

The *Ktu*$^{-/-}$ mice exhibited a complete loss of ciliary motility in tracheal and ventricular epithelia. This is consistent with the phenotype of respiratory cells taken from *KTU*-defective human PCD patients caused by loss-of-function *KTU* mutations (Omran et al., 2008). Among ciliary motility mutants reported thus far, the *Mdnah5*-knockout mouse has been well characterized and served as a model of human PCD (Ibanez-Tallon et al., 2002). *Mdnah5* encodes a heavy chain of outer dynein arms and a mutation of this gene was found in families of human PCD patients (Olbrich et al., 2002). In *Mdnah5*-mutant mice, the beat frequency of ependymal cilia is severely reduced, irregular and asynchronous, and hydrocephalus begins to emerge at P3-5. In *Ktu*$^{-/-}$ mice, hydrocephalus was detectable at P0, much earlier than in *Mdnah5* mutants. This difference in pathogenic timing could be explained by the severity of motility defects. While cilia are completely paralyzed in *Ktu*$^{-/-}$ mice, dynein mutants often retain residual ciliary motility although coherent CSF is not generated in brain ventricles (Olbrich et al., 2002). Since the *Ktu* mutation assures the complete loss of ciliary motility without disruption of ciliogenesis at least in the trachea and brain ventricle, the *Ktu*$^{-/-}$ mouse provides an ideal model to study the pathogenesis of human PCD and the assessment of of the effects of motility loss in ciliated organs.

Chapter 3: Contribution of ciliary motility to rotational polarity

Introduction

To create a coherent directional fluid flow in multicilated tissues, ciliated cells should be controlled by at least two types of planar polarity, termed rotational polarity and tissue-level polarity during their differentiation process (Fig. 10B, C). The former refers to the ciliary alignment within a cell and is manifested by the position of the basal foot, a structure on the basal body at the base of each cilium that points in the direction of effective stroke (Fig. 10A). The latter is an inter-cellular polarity which results from the coordination of the rotational polarity in all the multi-ciliated cells within a tissue. Since cilia disorientation was frequently reported in human PCD, understanding the relationship between ciliary motility and these polarities has been a subject of recent studies (De Iongh and Rutland, 1989; Rautiainen et al., 1990; Wallingford, 2010).

Previous reports have shown the complex relationship between ciliary motility and the establishment of ciliary orientation. First, in murine tracheal cilia, basal foots are oriented by the planar cell polarity (PCP) pathway by the time they are formed, before the onset of ciliary beating (Vladar et al., 2012). During subsequent development, ciliary orientation is refined. The involvement of cilia motility was not examined in these studies, raising the question as to what extent cilia motility contributes to the establishment of coordinated alignment of cilia in these tissues. Elaborate work with *Xenopus* skin and mouse brain ependymal cells has revealed a slightly different mechanism in the establishment of rotational polarity in these tissues. As blockage of ciliogenesis and downregulation of PCP components both result in disroientation of cilia, basal bodies are assumed to re-orient in one direction through coupling of ciliary-driven hydrodynamic forces and PCP-mediated planar polarity (Guirao et al., 2010; Mitchell et al., 2007). Although the principal mechanism is similar, the power balance between two

key determinants is different in the establishment of rotational polarity in these two examples.

Ciliary motility and the cilia-driven hydrodynamic force was suggested to have a supportive role in *Xenopus* skin ciliary alignment, while in mouse ependymal cells, it plays a dominant role in the decision of ciliary direction. Although these studies were well performed, they were carried out using IFT-mutant mice in which ciliogenesis was genetically blocked, leading to no protruding cilium. Because of this, the effect of ciliary loss and motility loss cannot be clearly separated. Furthermore, as discussed before, mouse models with genetically disrupted ciliary motility reported so far still retained residual ciliary motility. In addition, ciliary alignment has not been assessed in dynein mutant mice. Thus, the extent to which cilia motility is involved in this process in mammals has not yet been fully clarified. Here, in order to address the role of ciliary motility in the process of coordinated cilia alignment (rotational polarity), I analyzed the trachea and brain ventricles of *Ktu*$^{-/-}$.

Material and Methods

Whole mount immunohistochemistry

Mice were killed and brains were collected in ice-cold PBS. The lateral ventricle wall of the brain was dissected and immersed in 4% PFA at 4ºC overnight. Isolated trachea were opened longitudinally and fixed in 4% PFA overnight at 4ºC. When staining with □-tubulin, TritonX-100 was added to a final concentration of 0.1% or 0.5% during fixation. After serial washing with PBS (20 min x 3), samples were blocked with normal goat serum. Primary antibodies were diluted in PBS and incubated for 4ºC overnight. After serial washing with PBDT (30 min x 3), samples were incubated with secondary antibodies and rhodamine phalloidin for 4ºC overnight. Samples were trimmed and mounted with 50% glycerol/PBS after serial washing with PBDT. Confocal images were obtained using a LSM710 (Zeiss) microscope. Primary antibodies were used in following concentrations. Rabbit anti-Pericentrin pAb (1:300; Covance, PRB-432C), rabbit anti-Vangl1 pAb (1:300; Sigma, HPA025235).

Electron microscopy

Tissues were isolated in ice-cold PBS and fixed in pre-fixation solution (2.5 % glutaraldehyde, 4% PFA, 0.1M phosphate buffer (pH7.4)) overnight at 4ºC and trimmed. After a series of washing in 0.1M cacodylate buffer (pH7.4), samples were post-fixed in 1% OsO_4/ 0.1M cacodylate buffer for 2 h and dehydrated with a graded ethanol series. After replacing with methyl oxirane. Samples were embedded in epoxy resin (Nissin EM) and hardened at 60ºC. Samples were sectioned into 80-95nm thick. Ultrathin sections were coated with iridium and contrasted with lead citrate (TAAB). After several washes in Milli Q water, sections were dried and observed by electron

microscopy (JEOL).

Quantitative analysis of basal foot orientation

To quantify the alignment of cilia within each cell, the directionality of the basal foot was measured by standard protocols (Guirao et al., 2010; Hirota et al., 2010) with modifications. A basal line was drawn for each picture (Fig. 11B). For each basal foot, a vector connecting the center of the basal body and the protrusion of basal feet was drawn. The angle between this vector and the basal line was measured manually using ImageJ software (Fig. 11C). In brief, 7-14 basal feet were measured per cell and 30-40 cells from 2-3 mice were used for each analysis. Mean angle was calculated for each cell using Oriana 4.0 software. Mean angle was defined as mean ciliary direction (shown as 0^{o} in each circular plot graph). Deviation from the mean angle was measured for all of the basal feet analyzed (Fig. 11D). Deviation angles of the basal feet were pooled and plotted on a circular graph using Oriana 4.0 software (on average, 300 basal feet, 20-30 cells, 2-3 mice were used in each experiment).

Results

Translational, but not rotational polarity, is normally established in mutant mice.

In addition to rotational polaritiy and tissue-level polarity, there is a third polarity in brain ependymal cells (Fig. 10C). Unlike most multi-ciliated cells where cilia (or basal bodies) cover the entire apical surface, the surface of ependymal cells in the brain ventricle are only partially covered by clusters of cilia and the position of these clusters are normally polarized to one end, which is referred to as translational polarity. I first examined whether translational polarity is established normally in ventricles of *Ktu*$^{-/-}$ as well as wild-type littermates. In mutant ventricles, basal bodies stained by anti-pericentrin antibody migrated to the apical cell border by P10 as in the wild-type tissue (Fig. 12A). These results suggest that translational polarity is normally established in the absence of Ktu. However, the migration pattern of basal bodies in mutants was different from that in wild-type in the following two aspects. First, probably due to general growth retardation, the migration is slower than that of wild type. Second, in wild-type ventricles, basal bodies tend to be tightly packed forming a crescent shape during migration, but they migrate in a loosely packed form in mutant cells (data not shown). Nonetheless, consistent with polarized distribution of basal bodies, we observed the asymmetric localization of Vangl1, one of the core PCP proteins, in mutant ependymal cells. In both wild-type and *Ktu*$^{-/-}$ ependymal cells, Vangl1 localizes asymmetrically to the posterior cell cortex, forming a pattern commonly termed ‘‘crescent’’ (Fig 12B), indicating the normal establishment of translational polarity in the absence of ciliary motility.

We then examined the rotational polarity in brain ependymal cells. For this, we quantified ciliary orientation at P10 by scoring orientations of basal feet in TEM

sections. The mean angle of the basal foot projections was calculated for each cell. Deviation against the mean angle was then calculated for all basal feet analyzed and pooled onto a circular plot (for details, see M & M). As shown in Fig. 12C, basal feet of *Ktu*$^{-/-}$ mice pointed in random directions when compared to the basal feet of *Ktu*$^{+/+}$ mice that are aligned parallel to each other (Fig. 12C). Deviation angles of basal feet varied in mutant mice suggesting a rotational orientation defect (Fig. 12D). These results indicate that cilia motility is required for normal cilium orientation in brain ependymal cells.

Cilium orientation is not determined by ciliary motility in trachea epithelial cells.

I then examined the rotational polarity in trachea epithelial cells of mutant mice. A recent paper reported that the establishment of ciliary orientation is largely determined by the PCP pathway in the trachea but involvement of ciliary motility in this process has not yet been determined (Vladar et al., 2012). In the mouse tracheal epithelium, ciliogenesis initiates at E16 in the trachea (Toskala, 2005) and PCP-protein asymmetry emerges prior to the onset of ciliogenesis (Vladar et al., 2012). I first examined the localization of Vangl1 at P10 (Kunimoto et al., 2012; Vladar et al., 2012) and found that Vangl1 showed asymmetric distribution within the cell surface (cortex) in both wild-type and *Ktu*$^{-/-}$ mice (Fig. 13A), indicating that planar polarity is established normally in the absence of Ktu. I then examined the orientation of basal feet in tracheal epithelial cells by the method described above. Surprisingly, the orientation of basal feet in mutant cells at P10 was almost unidirectional similar to those in control littermates (Fig. 13B), indicating that the motility of cilia does not contribute to cilium orientation in the tracheal epithelium.

Discussion

It was recently reported that the rotational orientation of tracheal cilia is largely determined by the PCP pathway (Vladar et al., 2012). The tracheal epithelium exhibits a clear anterior-posterior polarity in which PCP components such as Vangl1 are asymmetrically localized in each cell. This tissue-level polarity is established by E14.5, and ciliogenesis and the formation of rotational polarity takes place in these molecularly polarized cells at E16.5 and onward. The timing in appearance of cellular and ciliary polarities supports the major contribution of the PCP pathway to initial cilium orientation. Once roughly oriented based on tissue-level polarity, cilium orientation is progressively refined at late embryonic and early neonatal (E17.5-P5) stages (Vladar et al., 2012). Like in other multiciliated epithelia (discussed below), this refinement was also thought to require ciliary motility-driven fluid flow. However, in *Ktu*$^{-/-}$, the refinement process appeared to normally take place, and at P10 the cilium orientation in mutant cells was indistinguishable from that in wild-type cells, suggesting that both initial orientation and the subsequent refinement process in tracheal cilia are independent of ciliary motility. If so, what mechanism drives the refinement process of the immotile cilia in *Ktu*$^{-/-}$? As *Ktu*$^{-/-}$ cells showed proper alignment, I suspect that multi cilia are able to sense extracellular cues albeit the loss of motility. Indeed there is emerging evidence that like primary cilia, motile cilia in the respiratory and reproductive tracts of humans and mice can also function as sensors to external cues such as mechanical and chemical ones (Guirao et al., 2010; Kamura et al., 2011; Shah et al., 2009). Interestingly, it has been reported that bi-directional fluid flow is produced in the trachea through fetal breathing movements during late embryonic development, a period when the refinement takes place (Fortin and Thoby-Brisson, 2009). Multi cilia in

Ktu$^{-/-}$ cells would sense this environmental flow. Further studies will be necessary to elucidate the mechanism responsible for the motility-independent refinement process in trachea.

In ependymal cells, the tissue-level and translational polarity was normally established in the absence of Ktu as indicated by the asymmetric distribution of Vangl1 and clustered cilia. However, rotational polarity was severely affected. Thus in contrast to trachea, alignment of multi cilia in ependymal cells depend on ciliary motility. These results are largely consistent with studies with IFT-mutant mice (Guirao et al., 2010; Mirzadeh et al., 2010). However, the ciliary orientation in *Ktu*$^{-/-}$ cells is not totally random but exhibits some bias (Fig. 12D). It was previously shown that IFT-mutant ependymal cells exhibit no bias in the orientation of basal body docking (Guirao et al., 2010). This discrepancy, again, could be explained by the sensing ability of motile cilia; cilia in *Ktu*$^{-/-}$ cells, albeit lack of motility, would sense the initial CSF flow which is generated by CSF secretion in the choroid plexus and absorption in the subarachnoid cisterns (Redzic et al., 2005). Taking together, my results from trachea and ependymal cells strengthen the idea that multi cilia are not merely a fluid generator but a perception hub for environmental cues.

Ktu$^{-/-}$ mice provide concrete evidence that the dependency of motility for the establishment of ciliary orientation varies among tissues. What is the biological significance of this variety? The generation of flow requires a collection of ciliated cells working in unison, and feedback between flow and refinement would direct reorienting cilia in response to changes that occur during and after ciliogenesis. In the case of brain ventricles and the *Xenopus* epidermis, the surface of tissues continuously and dramatically changes in shape during development and growth. For these tissues, the

continuous feedback loop through active beating needs to be functional to assure directional liquid flow on the surface. In the case of the trachea, however, one directional rostro-caudal axis is genetically determined for the future clearance of mucus and this does not change for life, thus trachea cilia may not need the motility-driven feedback loop. Possibly due to this characteristic feature of organ development, the dependency of ciliary motility may have differentiated. Hence the power balance between fluid flow and planar polarity in establishment of coordinated orientation of motile cilia may be determined by the stability of the tissue morphology during development (Fig. 14).

General Discussion

In my Ph.D. study, I characterized the murine Ktu *in vivo* and *in vitro* and showed that Ktu is specifically expressed in cells that have motile cilia. This is consistent with the previous report (Omran et al., 2008) (Chapter 1). Furthermore, the *in vitro* study showed continuous expression of Ktu, prior and post ciliogenesis. Then I produced *Ktu* knockout mouse which exhibited complete ciliary motility loss thus proved to be an ideal PCD model. *Ktu*$^{-/-}$ was found to exhibit completely immotile cilia leading to typical PCD phenotypes such as hydrocephalus and *situs inversus* (Chapter 2). Through the analysis of these knockout mice, I was able to address the relationship between the ciliary motility and the establishment of rotational polarity. In the brain ependymal cells, the rotational polarity is largely dependent on ciliary motility. On the contrary, ciliary motility plays a minor role in the trachea epithelial cells. These results reveal the tissue-specific dependency of ciliary motility for coordinated ciliary alignment (Chapter 3, Fig. 14). Thus my study is the first to directly address the effect of ciliary motility in the establishment of rotational polarity. Based on these findings, I propose that the balance of power between ciliary motility and planar polarity is determined by the stability of the tissue morphology. This notion is consistent with the previous studies of quail oviduct and mouse node cilia in which planar polarity plays a major role in the establishment of ciliary(Boisvieux-Ulrich et al., 1991).

Finally, I would like to describe my prospect in the future studies of this research field. The molecular mechanism of how fluid flow and ciliary motility re-orient cilia needs to be elucidated. The cytoskeletons (actin and microtubules) that are attached to the basal bodies are suggested to regulate ciliary re-orientation (Werner et al., 2011). Interestingly. microtubules are attached to the basal foot, whereas actin filaments are attached to the

opposite end, striated ciliary rootlet (Kunimoto et al., 2012; Vladar et al., 2012). Furthermore, it is known that Dvl2, a cytoplasmic effector of PCP pathway regulates rotational polarity in the *Xenopus* skin and mouse brain ependymal cilia (Hirota et al., 2010; Park et al., 2008). Thus it is assumed that Dvl2 transmits the extra-cellular cues into the cell and control cytoskeltons. It is reported that Dvl binds to Rho GTPase, a major regulator in actin dynamics (Park et al., 2008). In ciliated cell, Dvl2 is localized to the ciliary rootlet (Hirota et al., 2010) (Fig. 15). In *Ktu*$^{-/-}$, the localization of Dvl2 did not change significantly, suggesting that ciliary motility did not affect the localization of Dvl2 (data not shown). Further investigation should be necessary to examine the activation of Rho family downstream of ciliary motility and reorganization of the actin filaments. The involvement of microtubules in this process has not been examined so far.

In conclusion, my thesis study show that the generation of the uni-directional alignment of cilia within a cell is dependent on the ciliary motility to different levels in different tissues.

.

Figures

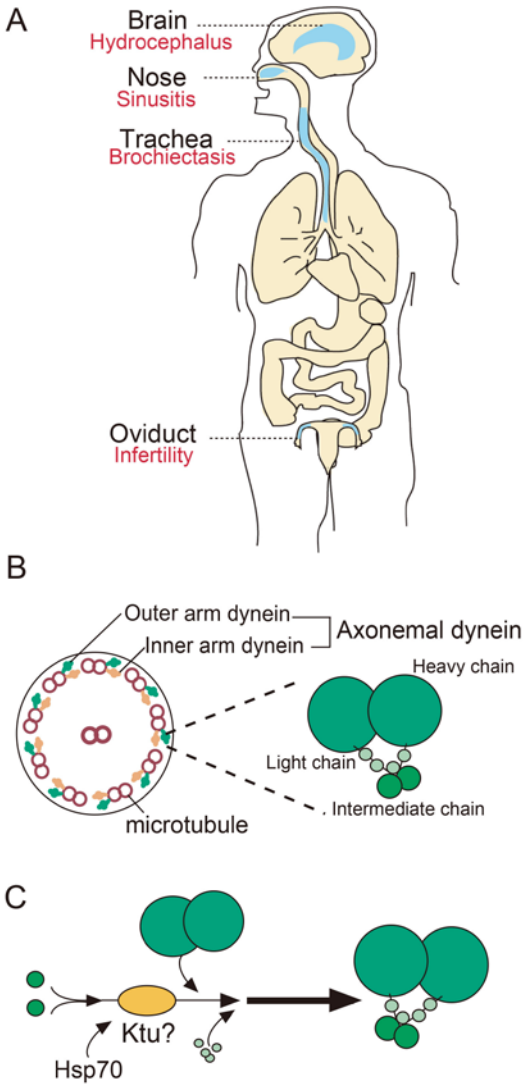

Fig. 1. Schematic picture of motile cilia structure

(A) Schematic picture of multiciliated tissues in human body. Red letters show PCD phenotypes in respective tissues. (B) Left: Transverse section of motile cilia representing 9+2 structure of microtubule circular orientation. Right: Detailed structure of microtubule associated dynein arms. (C) Hypothetical function of Ktu in the process of ourter arm dynein complex formation.

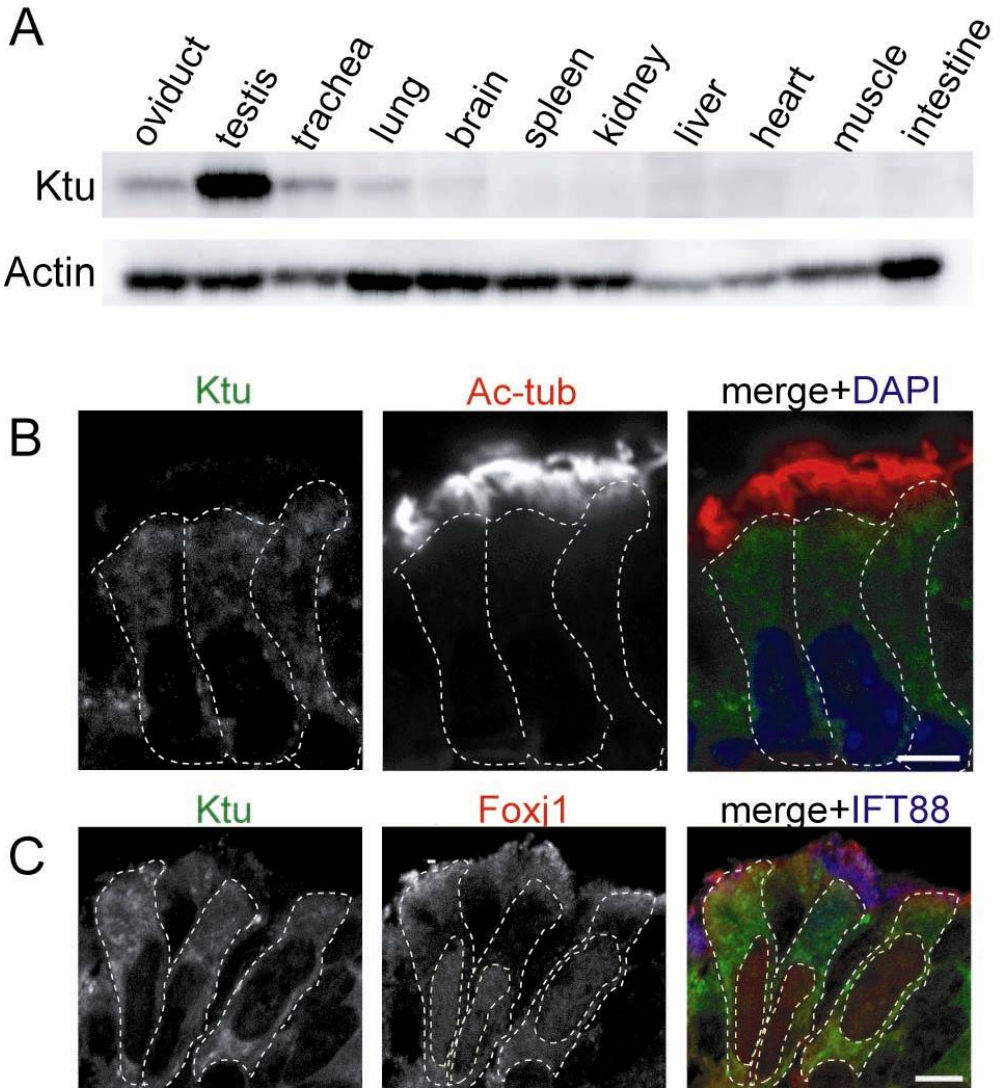

Fig. 2. Ktu is expressed in multiciliated tissues.

(A) Immunofluorescence of P14 mouse organs by anti-Ktu pAb. Expression of Ktu was detected in multiciliated/ flagellated tissues (oviduct, testis, trachea, brain). (B) Anti-Ktu pAb was double-immunolabeled with anti-acetylated α-tubulin mAb (Ac-tub, a cilia marker, B), (C) withanti-Foxj1 mAb (multiciliated cell marker) in trachea epithelial cells,.

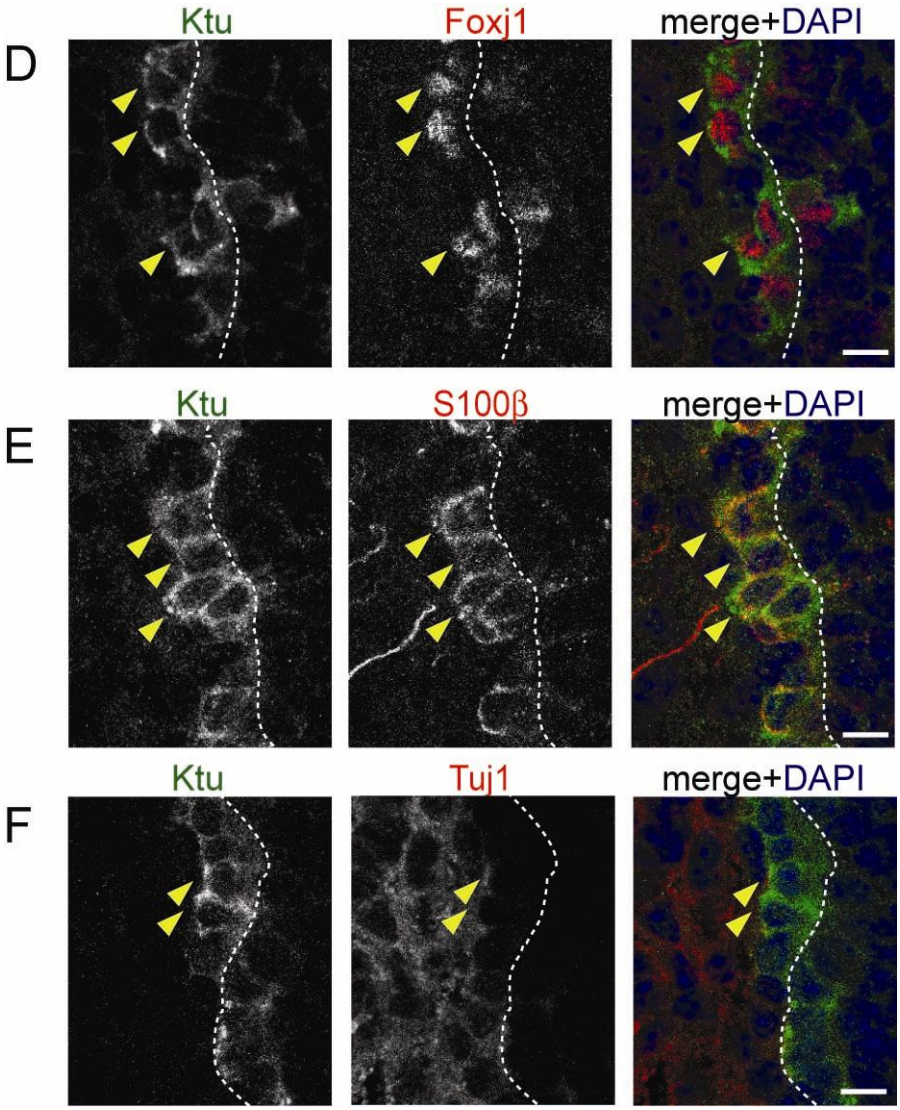

Fig. 2. (Continued)

(D-F) Expression of Ktu in mouse ependymal cells in lateral brain ventricles was analyzed by immunofluorescence using anti-Ktu pAb (green) and anti-Foxj1 mAb (red, multiciliated cell marker, D), S100β (red, ependymal cell marker, E) , and Tuj1 (red, neuronal marker, F). Ktu was detected in Foxj1-postive cells, indicating that it is expressed in multiciliated cells. Ktu also co-localized with S100β but did not co-localize with neuronal marker Tuj1 in the lateral ventricles (yellow arrowheads). DAPI is the marker for nuclei (blue). Dotted lines represent the walls of the ventricle lumen. Scale bars: 5 μm in B, C; 10 μm in D, E, F.

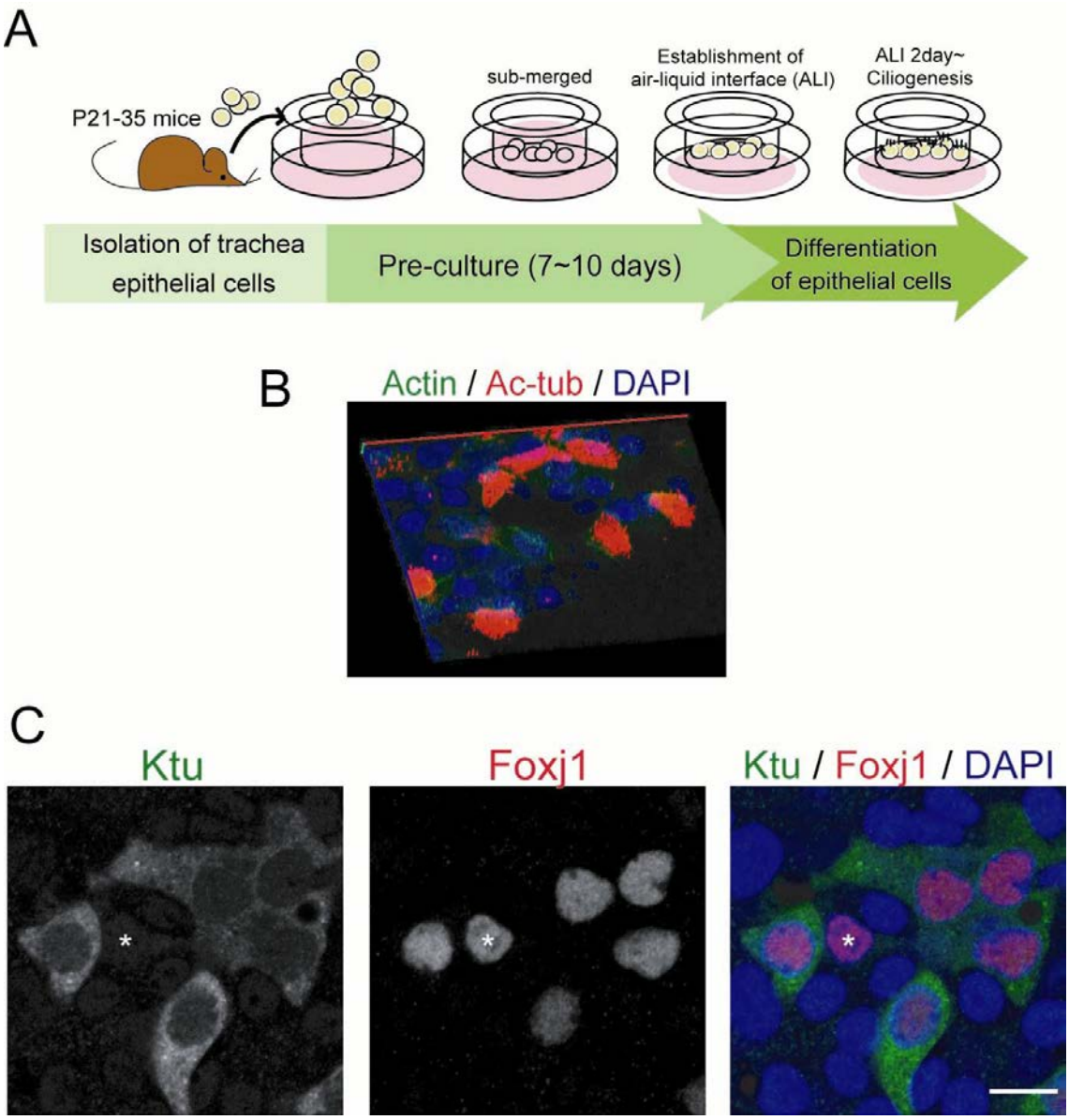

Fig. 3. In vitro studies of ciliogenesis using MTEC

(A) Schematic illustration of the production of MTEC. (B) A 3D reconstruction of confocal microscopy images showing normal ciliogenesis in the MTEC culture system. MTEC are immunolabeled with actin (green, cell border) and acetylated α-tubulin (Ac-tub, red) and DAPI (blue, nucleus). (C) Ktu (green) is expressed in the Foxj1-positive cells (red). The asterisk shows a Foxj1 (+) Ktu (-) cell. Scale bars: 10 μm in B.

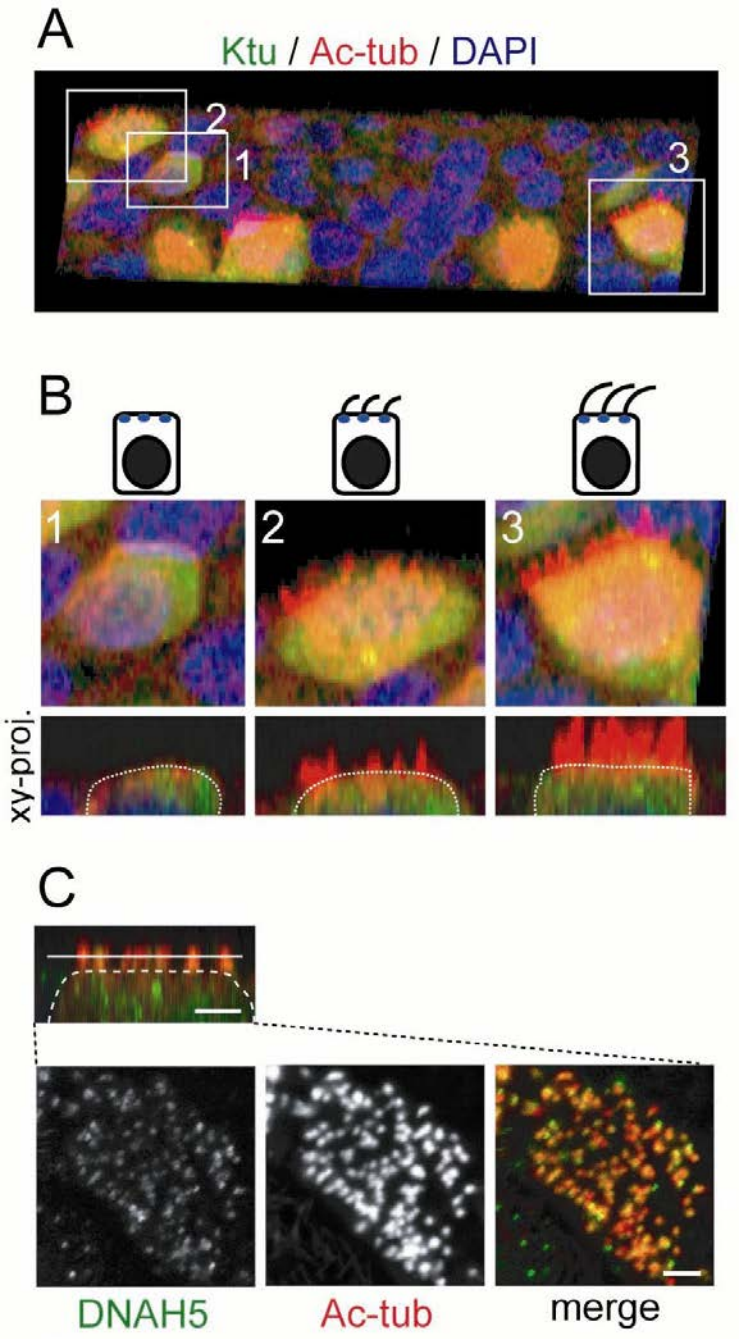

Fig. 4. Localization of Ktu during ciliogenesis

(A) A 3D reconstruction of the MTEC immunolabeled with Ktu (green) and acetylated α-tubulin (Ac-tub, red). (B) Cells at different ciliogenesis stages boxed in A. 1: pre-ciliogenesis period, 2: early-ciliogenesis period, 3: cilia elongation period. Serial confocal images projected in the x-z plane are shown in the lower panels. Ktu is expressed widely within the cytoplasm before and during ciliogenesis. (C) DNAH5 (axonemal dynein protein) localized to cilia at an early ciliogenesis stage. Scale bars: 2 μm in C.

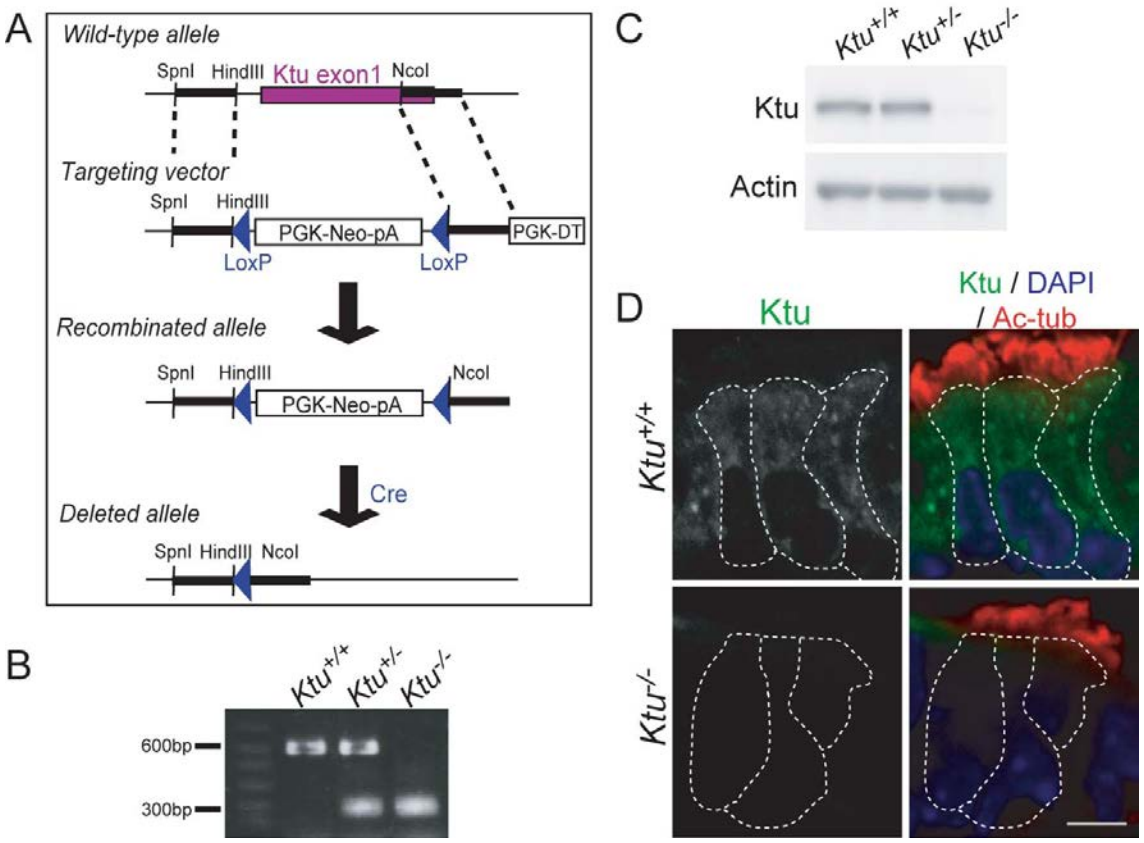

Fig. 5. Generation of *Ktu* knockout mouse.

(A) Construction of the wild-type allele, targeting vector, recombinated allele, and deleted allele of the mouse *Ktu* gene. The 1st exon was recombinated with the targeting vector. The recombinated allele was then deleted through Cre recombinase. (B) Genotype of $Ktu^{-/-}$ littermates by PCR. (C) Western blot analysis of Ktu from mouse testis. Ktu protein (120 kDa) is depleted in the homozygous knockout mouse. (D) Indirect immunofluorescence of trachea epithelial cells from P7 mice using anti-Ktu pAb and anti-acetylated α-tubulin mAb. Cytoplasmic expression of Ktu (green) was lost in the $Ktu^{-/-}$. White dotted lines demarcate individual cells. Scale bar: 5 μm.

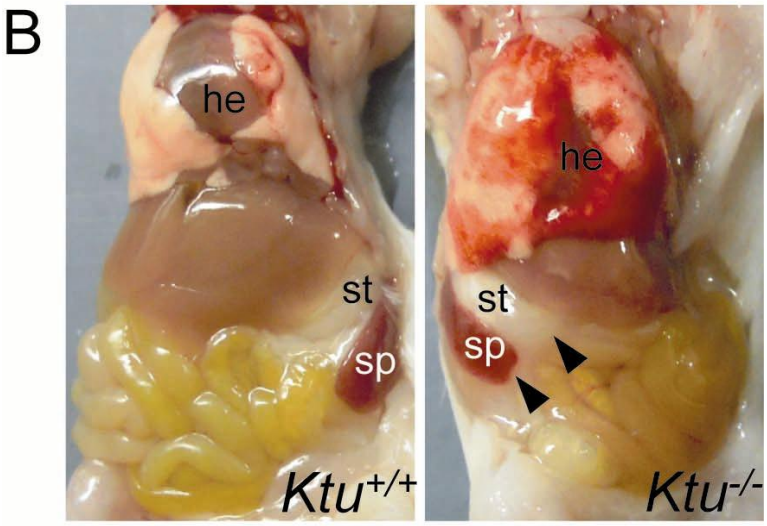

C

normal	*situs inversus*	total
26	17	43
(60%)	(40%)	(100%)

Fig. 6. Ktu knockout mice show primary ciliary dyskinesia

(A) *Ktu*$^{+/+}$and *Ktu*$^{-/-}$ littermates (P14). *Ktu*$^{-/-}$ shows growth defect. (B) Reversal of organ translocation (*situs inversus totalis*) in *Ktu*$^{-/-}$ (P14). Arrowheads indicate reversed localization of stomach and spleen. he, heart; st, stomach; sp, spleen. (C) Ratio of situs inversus totalis within *Ktu*$^{-/-}$ mice observed at P3.

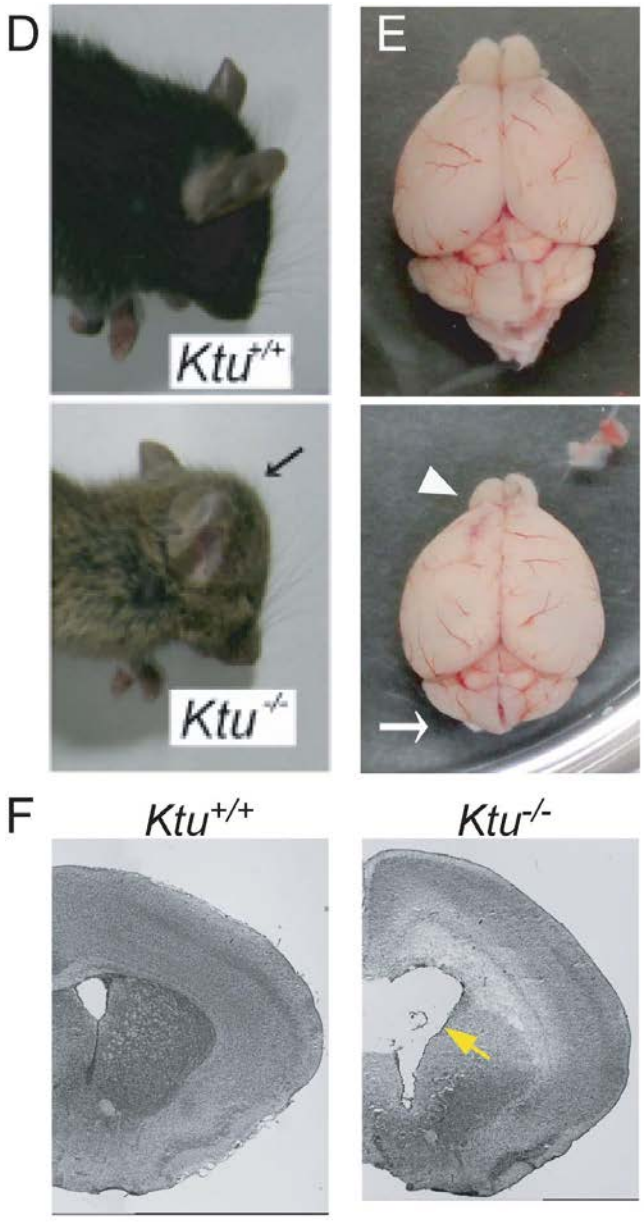

Fig. 6. (Continued)

(D) The *Ktu*$^{-/-}$ develops hydrocephalus and exhibits a dome-shaped head at P14 (arrow). (E) The olfactory bulb is diminished (white arrowhead) and the cerebellum is pressed in *Ktu*$^{-/-}$ (white arrow). (F) Coronal section of P14 brains stained with Haematoxylin and Eosin (H&E) staining. The lateral ventricle is enlarged in *Ktu*$^{-/-}$ (yellow arrow).

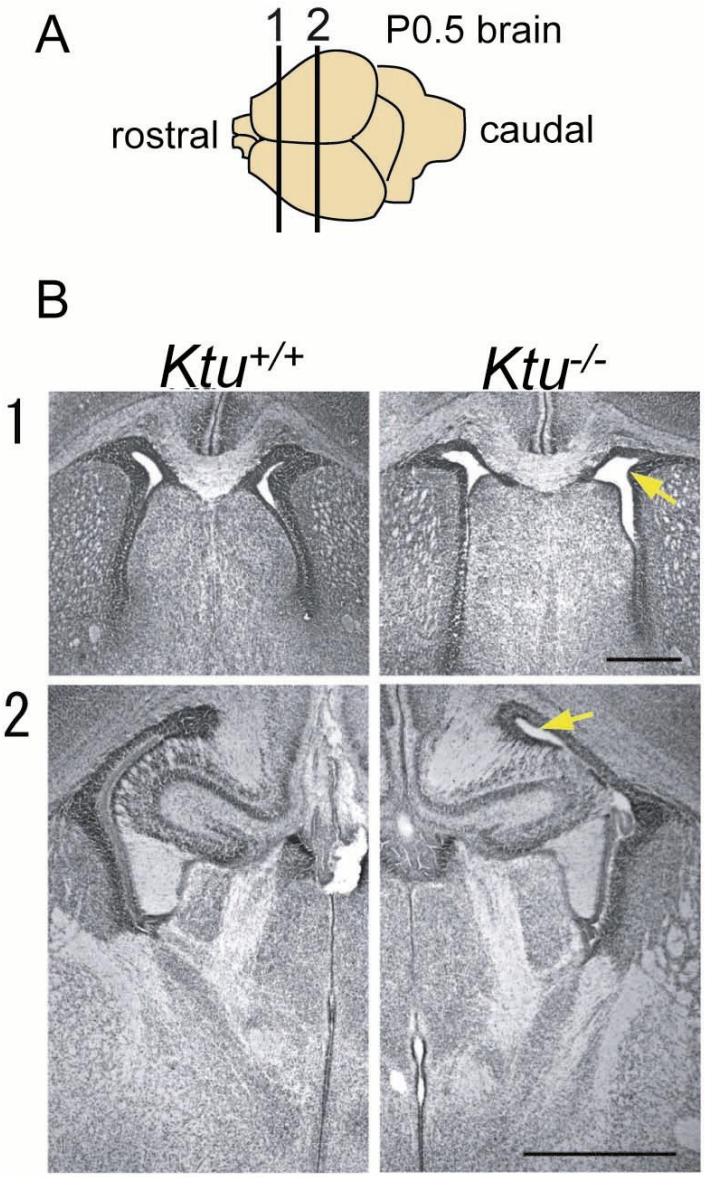

Fig. 7. Hydrocephalus initiates between E18-P0

(A)Schematic picture of the section position of the P0.5 brain shown in B. (B) Coronal sections of P0.5 *Ktu*$^{+/+}$ (left) and the *Ktu*$^{-/-}$ (right) brains. In both rostral (1) and caudal (2) positions, lateral ventricles are enlarged (yellow arrows). Haematoxylin and eosin (H&E) staining. The lateral ventricle is enlarged in *Ktu*$^{-/-}$ (yellow arrows).

Scale bar: 1 mm.

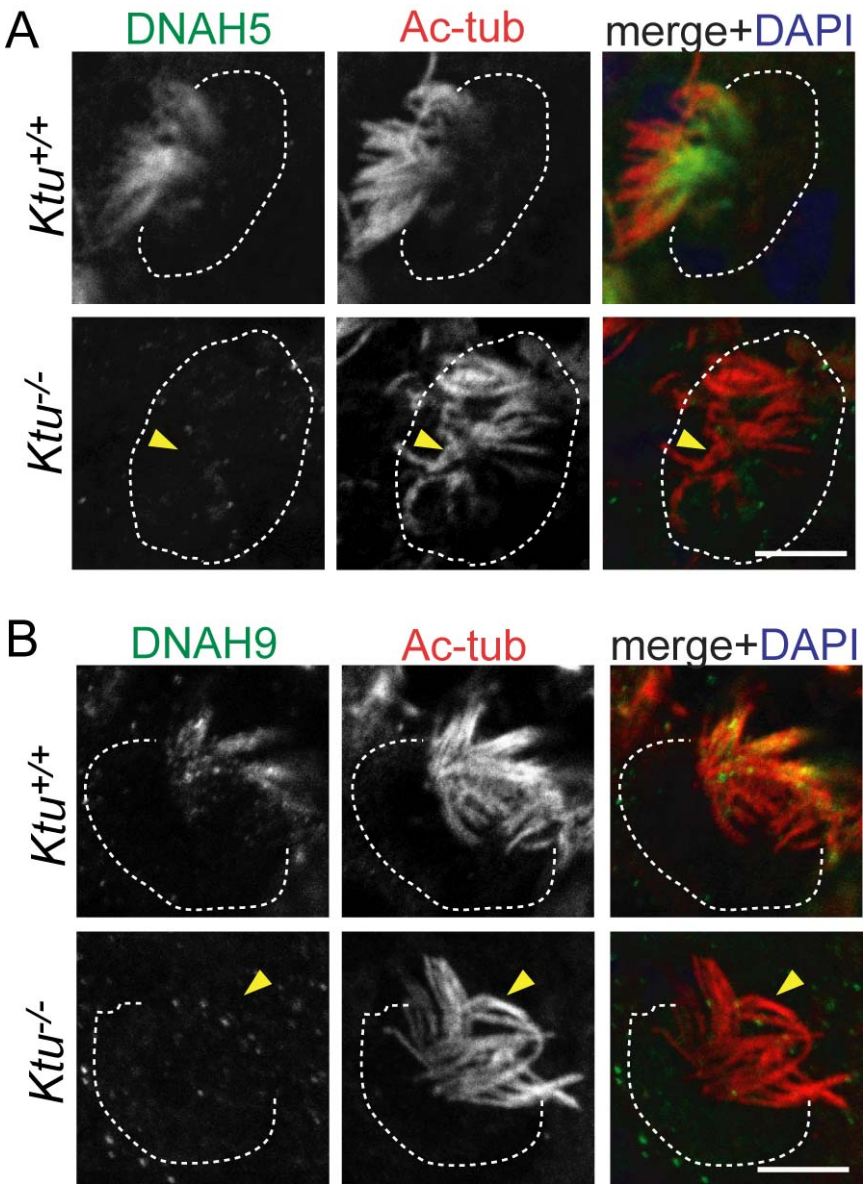

Fig. 8. Absence of axonemal dynein components in the *Ktu*$^{-/-}$ in brain ependyma
(A) Ciliary localization of axonemal dynein was visualized by immunofluorescence of ependymal cells in P7 lateral ventricles with anti-DNAH5 pAb and anti-acetylated α-tubulin (Ac-tub, cilia marker) mAb. (B) Double-immunolabeling with anti-DNAH9 pAb and anti-acetylated α-tubulin mAb (Ac-tub).

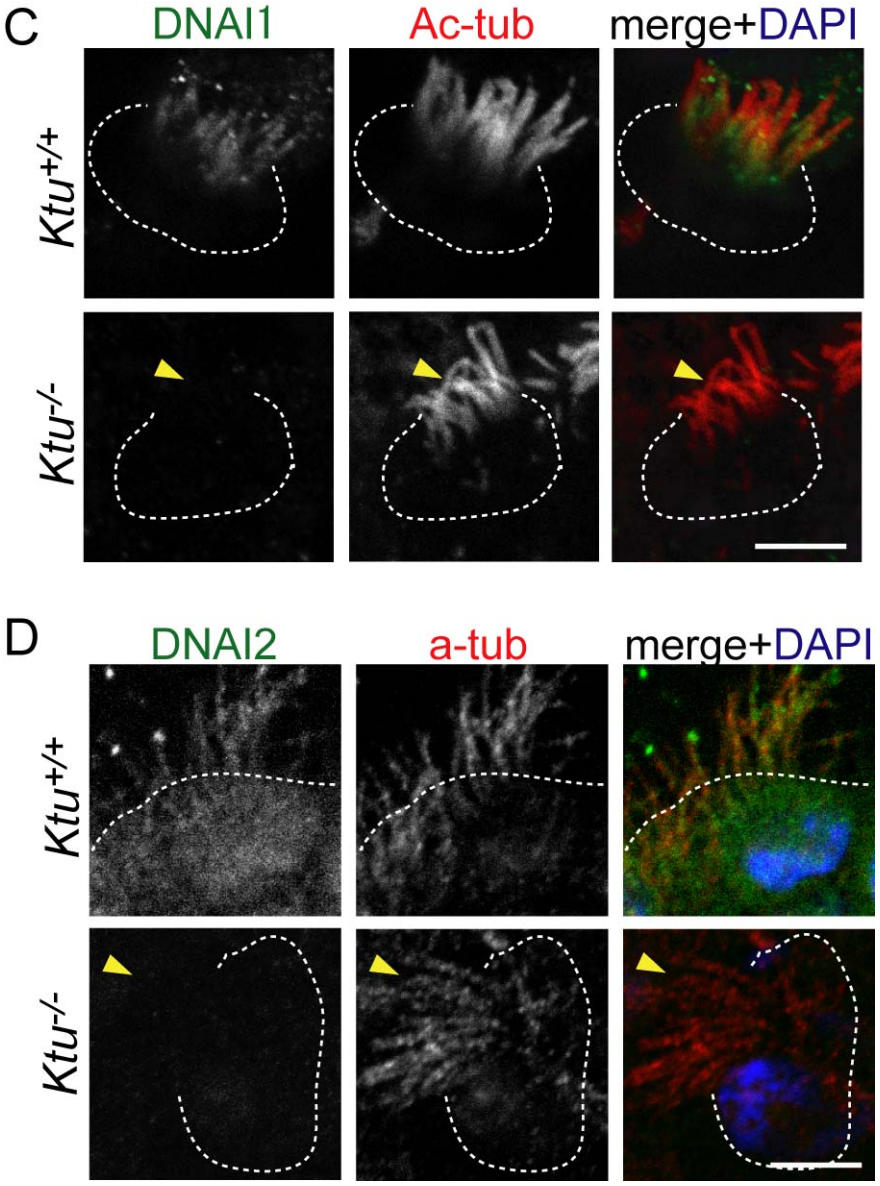

Fig. 8. (Continued)

(C) Indirect immunofluorescence using anti-DNAI1 pAb and anti-acetylated α-tubulin mAb (Ac-tub). (D) Immunohistochemistry using anti-DNAI2 mAb and anti-α-tubulin pAb. In *Ktu*$^{+/+}$, DNAH5 (green, A), DNAH9 (green, B), DNAI1 (green, C) and DNAI2 (green, D) is expressed along the ciliary axoneme (red), but in *Ktu*$^{-/-}$, none of them is detected (yellow arrowheads). The white dotted lines indicate the surface of the cells.

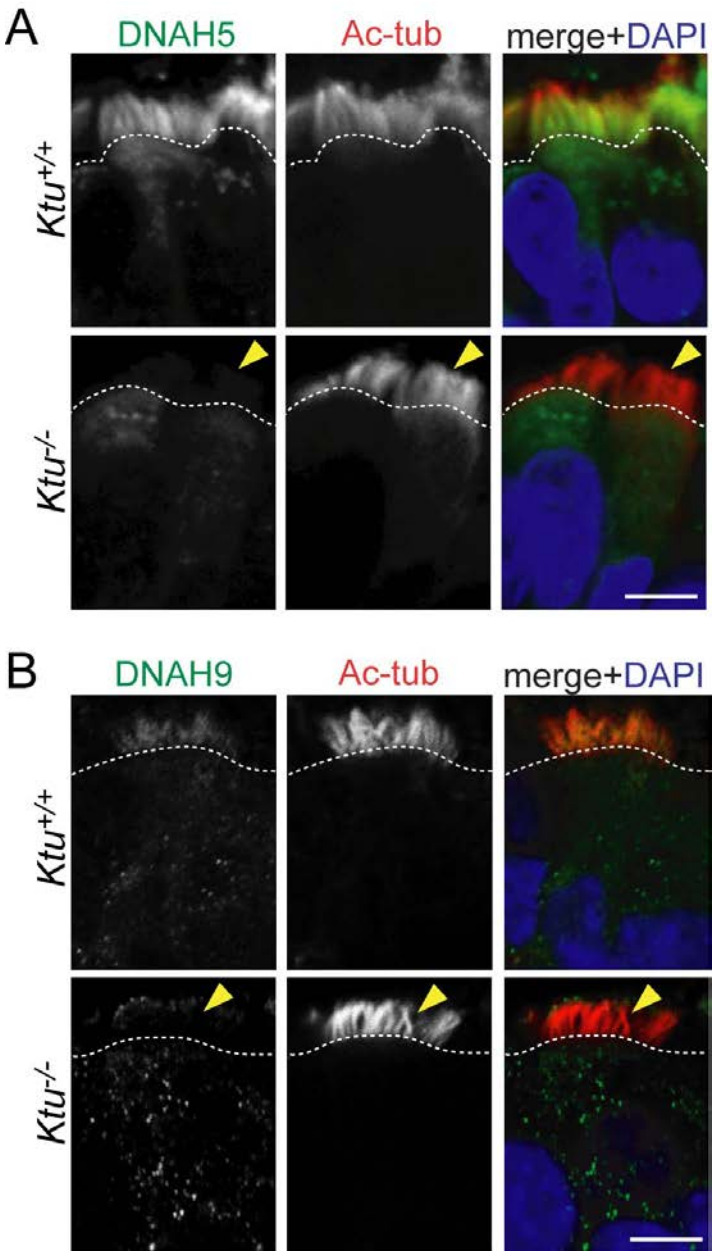

Fig. 9. Absence of axonemal dynein components in the *Ktu*$^{-/-}$ multicilia of trachea epithelial cells

(A) Ciliary localization of dynein components was visualized by immunofluorescence of P7 trachea epithelial cells with anti-DNAH5 pAb and anti-acetylated α-tubulin (Ac-tub, cilia marker) mAb. (B) Immunohistochemistry using anti-DNAH9 pAb and anti-acetylated α-tubulin In *Ktu*$^{+/+}$, DNAH5 (green, A), DNAH9 (green, B) is expressed along the ciliary axoneme (red), but in *Ktu*$^{-/-}$, DNAH5 was absent from the axoneme (yellow arrowheads, A). Similarly, signal of DNAH9 was lost from the ciliary base yellow arrowheads, B). The white dotted lines indicate the surface of the cells.

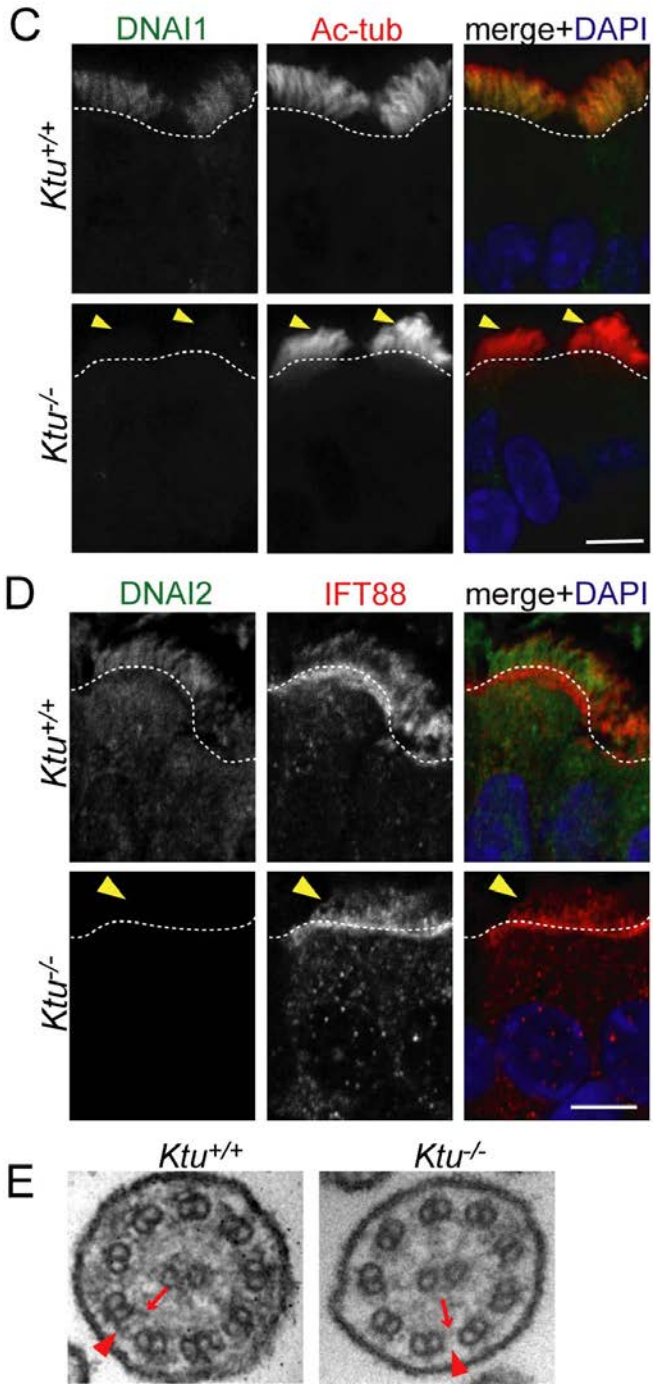

Fig. 9. (Continued)

Immunohistochemistry of trachea epithelial cells with (C) anti-DNAI1 pAb and anti-Ac-tub mAb. (D) anti-DNAI2 mAb and anti-α-tubulin pAb. In *Ktu*$^{+/+}$, DNAI1 (green, C) and DNAI2 (green, D) is expressed along the ciliary axoneme (red), but in *Ktu*$^{-/-}$, none of them are detected (yellow arrowheads) in the axoneme (E) Cross-section of trachea ciliary axoneme visualized by transmission electron microscope. Cilia of *Ktu*$^{-/-}$ lack inner arm dynein (red arrow) and outer arm dynein (red arrow head),

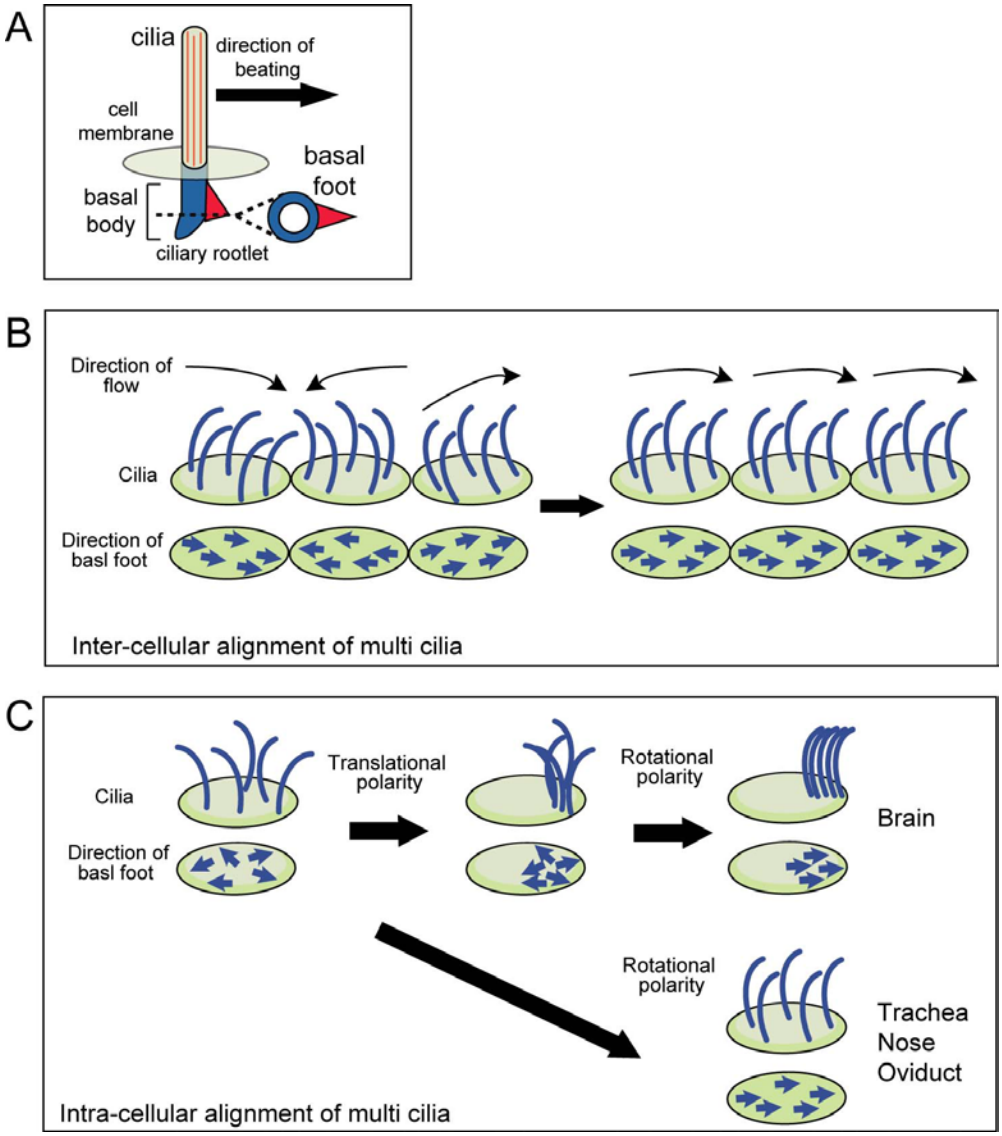

Fig. 10. Schematic view of coordinated ciliary alignment within the cell and among cells

(A) Schematic illustration of the motile cilium and its basal structure. The directionality of ciliary beat corresponds to the direction of the basal foot. Ciliated cells align their cilia to beat in a uni-directional manner in the tissue. (B) The coordinated alignment of cilia between cells (inter-cellular alignment) is called as the tissue-level polarity. (C) Coordinated alignment of cilia also exists within the cell (rotational polarity). Basal foot aligns in the same direction during/ after ciliogenesis in each cell. In brain ependyma, cilia patches migrate toward the one side of the cell (translational polarity) before the establishment of rotational polarity. Other ciliated cells harbor cilia in a uniform manner within the cell surface.

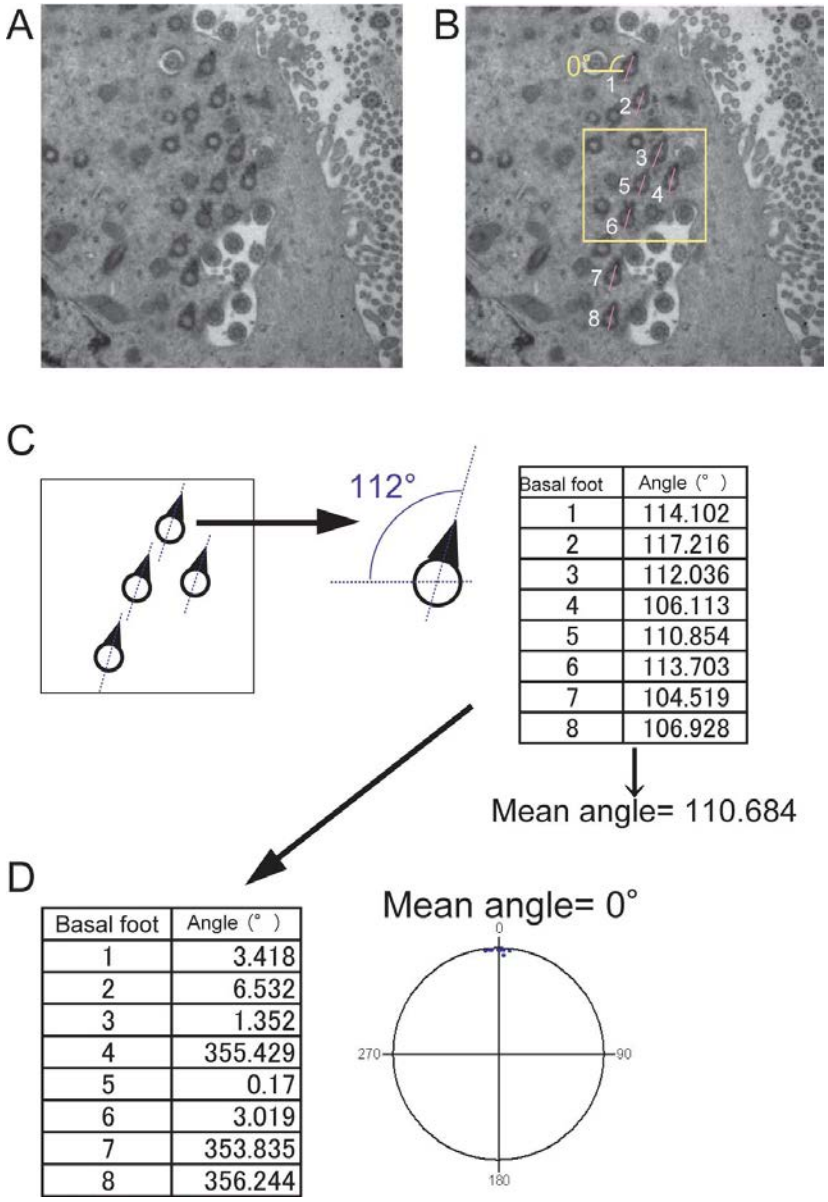

Fig. 11. Quantitive analysis of basal foot orientation

To quantify the alignment of cilia in each cell, the directionality of the basal foot was measured. (A) TEM section of trachea epithelial cells cut in the basal position of cilia. The basal foot are shown in dense arrow-like structure. (B) A basal line was drawn for each picture (yellow line). For each basal foot, a vector connecting the center of the basal body and the protrusion of basal feet was drawn (pink line). (C) Schematic illustration of basal foot that are boxed in B. A basal line that is parallel to the base of the picture was drawn for each picture taken. The angle between each vector and the basal line was measured manually using ImageJ software. The mean angle was calculated for each cell using Oriana 4.0 software. (D) The mean angle was defined as the mean ciliary direction (0º).

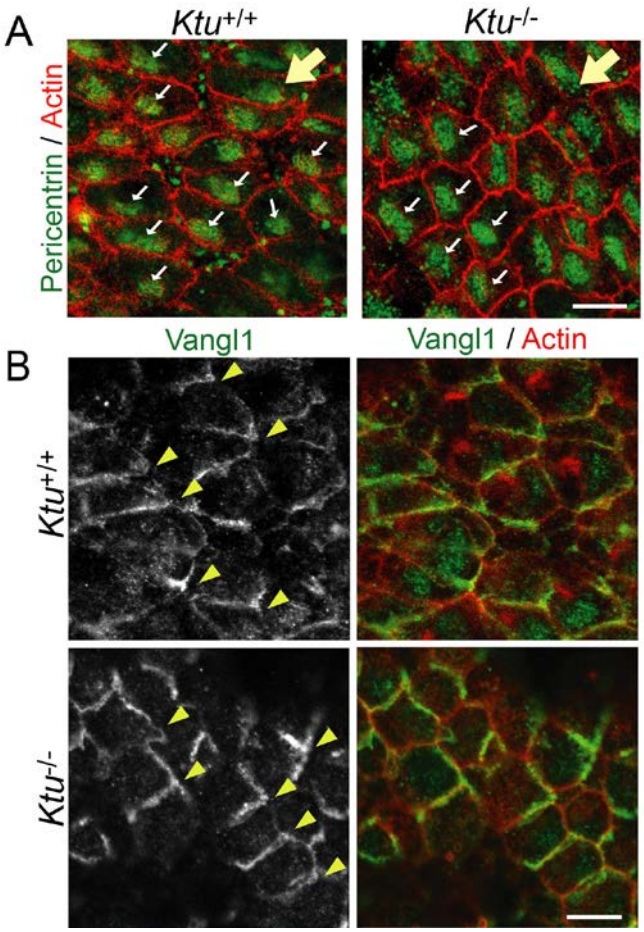

Fig. 12. Loss of cilia motility affects alignment of basal bodies in brain ependymal cells.

(A) Double-–label immunohistochemistry of P10 lateral ventricles with anti-Pericentrin pAb (green, basal body marker) and anti-Actin pAb (red, cell border marker). Basal bodies (arrows) migrated toward the anterior side of ependymal cells (yellow arrow) in *Ktu*$^{+/+}$ (left). Migration of basal bodies was unaffected in *Ktu*$^{-/-}$ (right). (B) Asymmetrical localization of Vangl1 (green) immunolabeled with actin (red) in the brain ependymal cells (P10). Asymmetrical localization of Vangl1 was retained in *Ktu*$^{-/-}$ (yellow arrowheads). Scale bars: 10 μm in A, B.

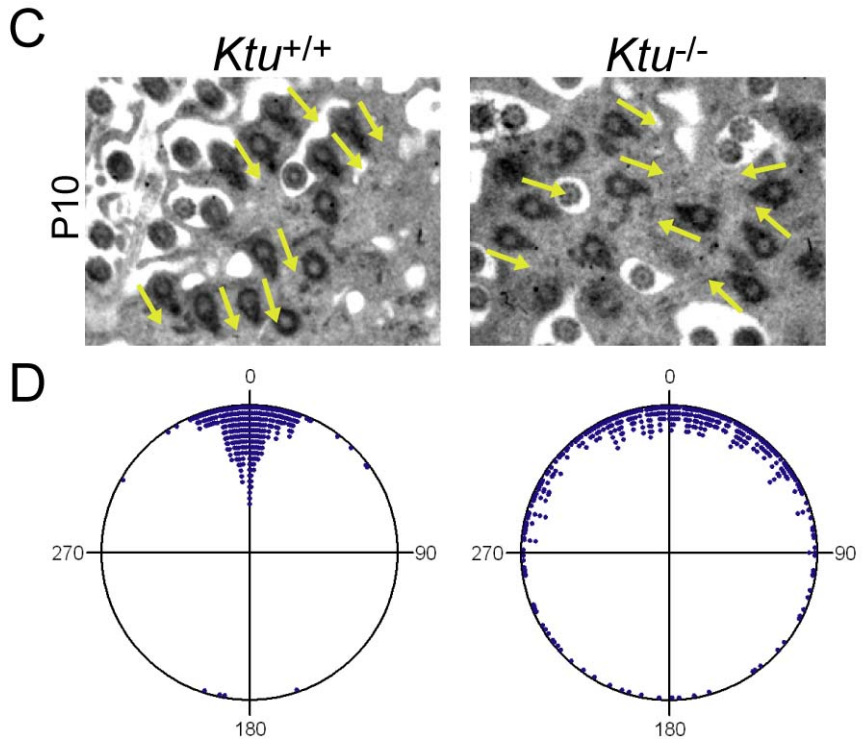

Fig. 12. (Continued)

(C) TEM sections of P10 brain ependymal cells. Unidirectional alignment of basal feet was observed in *Ktu*$^{+/+}$ (rotational polarity). Rotational polarity was disrupted in *Ktu*$^{-/-}$. Directions of basal foot are shown by yellow arrows. (D) Circular plots of deviation angles of the basal feet. Mean angles are pointed to 0. (*Ktu*$^{+/+}$, 284 basal feet in 38 cells from 3 mice; *Ktu*$^{-/-}$, 350 basal feet in 39 cells from 2 mice).

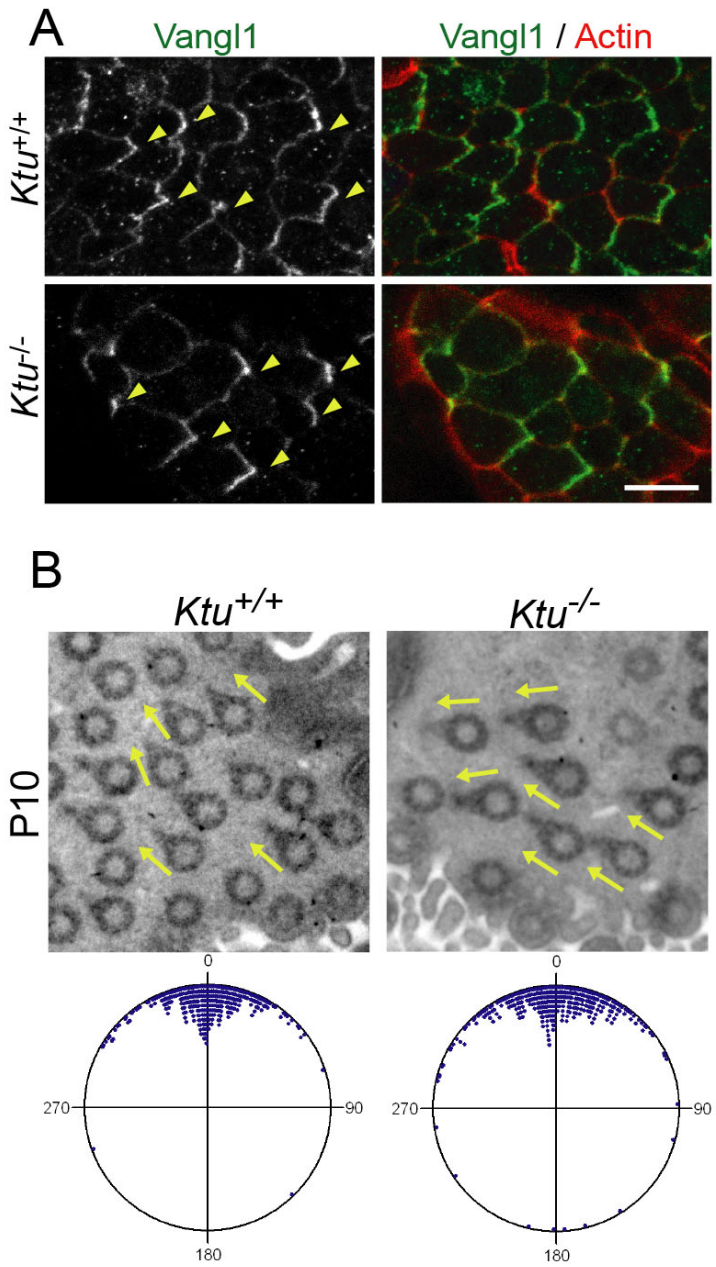

Fig. 13. Alignment of basal feet in trachea epithelial cells is unaffected in a Ktu knockout mouse

(A) Trachea epithelial cells from P10 mice were immnunolabeled with anti-Vangl1 pAb (green) and anti- actin pAb (red). Posterior-specific localization of Vangl1 was established in *Ktu*$^{-/-}$ as well as *Ktu*$^{+/+}$ (yellow arrowheads). Scale bar: 10 μm. (B) TEM sections of P10 trachea epithelial cells of *Ktu*$^{+/+}$ (left) and *Ktu*$^{-/-}$ (right). Directionality of the basal feet is established in the *Ktu*$^{-/-}$ (yellow arrows). Circular plots of deviation angles of the basal feet (bottom). Mean angles are pointed at 0. (*Ktu*$^{+/+}$, 319 basal feet in 31 cells from 2 mice; *Ktu*$^{-/-}$, 341 basal feet in 29 cells from 3 mice.

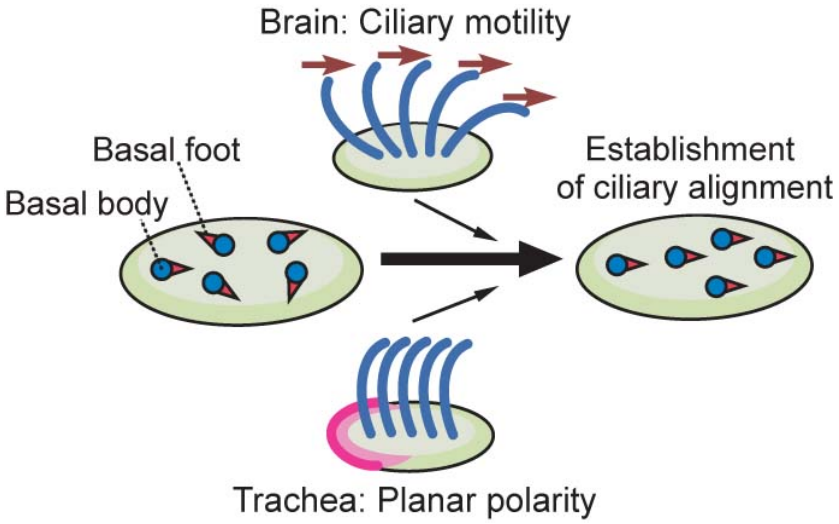

Fig. 14. Schematic picture of the establishment of rotional polarity in different tissues

Basal foot are aligned within the cell (rotational polarity). The major determinant of rotational polarity is the ciliary motility in the brain ependyma and planar polarity in trachea epithelial cells.

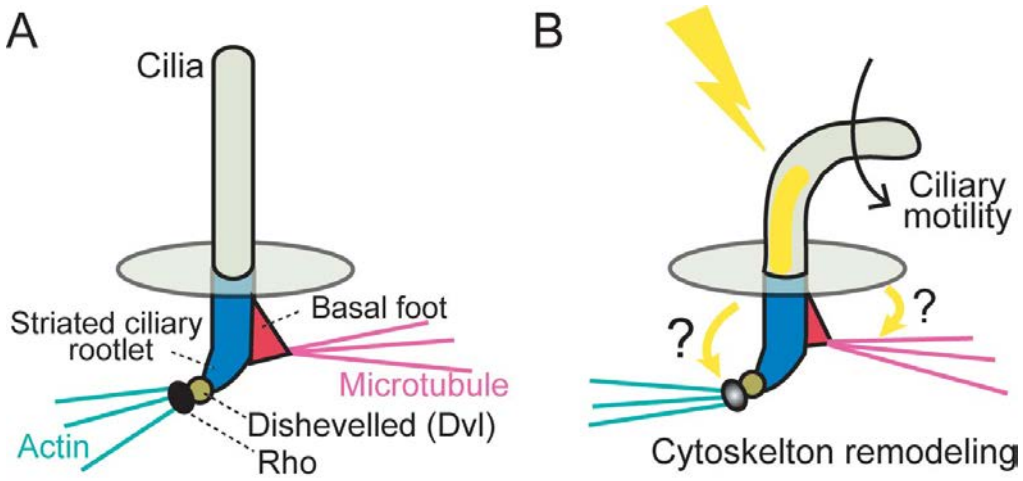

Fig. 15. Hypothetical model of ciliary re-orientation through ciliary motility

Actin filaments and microtubules are attached to striated ciliary rootlet and basal foot respectively. The Dvl-Rho complex is known to regulate actin remodeling. Ciliary motility may activate Dvl-Rho dependent actin remodeling pathway and reorient cilia.

Reference

Blatt, E. N., Yan, X. H., Wuerffel, M. K., Hamilos, D. L. and Brody, S. L. (1999). Forkhead transcription factor HFH-4 expression is temporally related to ciliogenesis. *Am. J. Respir. Cell Mol. Biol.* **21**, 168-176.

Boisvieux-Ulrich, E., Sandoz, D. and Allart, J. P. (1991). Determination of ciliary polarity precedes differentiation in the epithelial cells of quail oviduct. *Biol. Cell* **72**, 3-14.

Chilvers, M. A., Rutman, A. and O'Callaghan, C. (2003). Ciliary beat pattern is associated with specific ultrastructural defects in primary ciliary dyskinesia. *J. Allergy Clin. Immunol.* **112**, 518-524.

De Iongh, R. and Rutland, J. (1989). Orientation of respiratory tract cilia in patients with primary ciliary dyskinesia, bronchiectasis, and in normal subjects. *Journal of Clinical Pathology* **42**, 613-619.

de Iongh, R. U. and Rutland, J. (1995). Ciliary defects in healthy subjects, bronchiectasis, and primary ciliary dyskinesia. *American Journal of Respiratory and Critical Care Medicine* **151**, 1559-67.

Dirksen, E. R. (1991). Centriole and basal body formation during ciliogenesis revisited. *Biology of the Cell* **72**, 31-38.

Duquesnoy, P., Escudier, E., Vincensini, L., Freshour, J., Bridoux, A.-M., Coste, A., Deschildre, A., de Blic, J., Legendre, M., Montantin, G. et al. (2009). Loss-of-Function Mutations in the Human Ortholog of Chlamydomonas reinhardtii ODA7 Disrupt Dynein Arm Assembly and Cause Primary Ciliary Dyskinesia. *The American Journal of Human Genetics* **85**, 890-896.

Fliegauf, M., Benzing, T. and Omran, H. (2007). When cilia go bad: cilia defects and ciliopathies. *Nat Rev Mol Cell Biol* **8**, 880-893.

Fortin, G. and Thoby-Brisson, M. (2009). Embryonic emergence of the respiratory rhythm generator. *Respiratory Physiology & Neurobiology* **168**, 86-91.

Fowkes, M. E. and Mitchell, D. R. (1998). The role of preassembled cytoplasmic complexes in assembly of flagellar dynein subunits. *Mol. Biol. Cell* **9**, 2337-2347.

Guirao, B., Meunier, A., Mortaud, S., Aguilar, A., Corsi, J.-M., Strehl, L., Hirota, Y., Desoeuvre, A., Boutin, C., Han, Y.-G. et al. (2010). Coupling between hydrodynamic forces and planar cell polarity orients mammalian motile cilia. *Nat Cell Biol* **12**, 341-350.

Hackett, B. P. (1995). Primary structure of hepatocyte nuclear factor/forkhead homologue 4 and characterization of gene expression in the developing respiratory and reproductive epithelium. *Proc. Natl. Acad. Sci. USA* **92**, 4249-4253.

Hagiwara, H., Ohwada, N. and Takata, K. (2004). Cell Biology of Normal and Abnormal

Ciliogenesis in the Ciliated Epithelium. In *International Review of Cytology*, vol. Volume 234, pp. 101-141: Academic Press.

Hirota, Y., Meunier, A., Huang, S., Shimozawa, T., Yamada, O., Kida, Y. S., Inoue, M., Ito, T., Kato, H., Sakaguchi, M. et al. (2010). Planar polarity of multiciliated ependymal cells involves the anterior migration of basal bodies regulated by non-muscle myosin II. *Development* **137**, 3037-3046.

Ibanez-Tallon, I. (2004). Dysfunction of axonemal dynein heavy chain Mdnah5 inhibits ependymal flow and reveals a novel mechanism for hydrocephalus formation. *Hum. Mol. Genet.* **13**, 2133-2141.

Ibanez-Tallon, I., Gorokhova, S. and Heintz, N. (2002). Loss of function of axonemal dynein Mdnah5 causes primary ciliary dyskinesia and hydrocephalus. *Hum. Mol. Genet.* **11**, 715-721.

Jacquet, B. V., Salinas-Mondragon, R., Liang, H., Therit, B., Buie, J. D., Dykstra, M., Campbell, K., Ostrowski, L. E., Brody, S. L. and Ghashghaei, H. T. (2009). FoxJ1-dependent gene expression is required for differentiation of radial glia into ependymal cells and a subset of astrocytes in the postnatal brain. *Development* **136**, 4021-4031.

Kamura, K., Kobayashi, D., Uehara, Y., Koshida, S., Iijima, N., Kudo, A., Yokoyama, T. and Takeda, H. (2011). Pkd1l1 complexes with Pkd2 on motile cilia and functions to establish the left-right axis. *Development* **138**, 1121-1129.

Kunimoto, K., Yamazaki, Y., Nishida, T., Shinohara, K., Ishikawa, H., Hasegawa, T., Okanoue, T., Hamada, H., Noda, T., Tamura, A. et al. (2012). Coordinated Ciliary Beating Requires Odf2-Mediated Polarization of Basal Bodies via Basal Feet. *Cell* **148**, 189-200.

Loges, N. T., Olbrich, H., Becker-Heck, A., Hテ、ffner, K., Heer, A., Reinhard, C., Schmidts, M., Kispert, A., Zariwala, M. A., Leigh, M. W. et al. (2009). Deletions and Point Mutations of LRRC50 Cause Primary Ciliary Dyskinesia Due to Dynein Arm Defects. *The American Journal of Human Genetics* **85**, 883-889.

Loges, N. T., Olbrich, H., Fenske, L., Mussaffi, H., Horvath, J., Fliegauf, M., Kuhl, H., Baktai, G., Peterffy, E., Chodhari, R. et al. (2008). DNAI2 Mutations Cause Primary Ciliary Dyskinesia with Defects in the Outer Dynein Arm. *The American Journal of Human Genetics* **83**, 547-558.

Mirzadeh, Z., Han, Y.-G., Soriano-Navarro, M., Garcia-Verdugo, J. M. and Alvarez-Buylla, A. (2010). Cilia Organize Ependymal Planar Polarity. *The Journal of Neuroscience* **30**, 2600-2610.

Mitchell, B., Jacobs, R., Li, J., Chien, S. and Kintner, C. (2007). A positive feedback mechanism governs the polarity and motion of motile cilia. *Nature* **447**, 97-101.

Mitchison, H. M., Schmidts, M., Loges, N. T., Freshour, J., Dritsoula, A., Hirst, R. A.,

O'Callaghan, C., Blau, H., Al Dabbagh, M., Olbrich, H. et al. (2012). Mutations in axonemal dynein assembly factor DNAAF3 cause primary ciliary dyskinesia. *Nat Genet* **44**, 381-389.

Olbrich, H., Haffner, K., Kispert, A., Volkel, A., Volz, A., Sasmaz, G., Reinhardt, R., Hennig, S., Lehrach, H., Konietzko, N. et al. (2002). Mutations in DNAH5 cause primary ciliary dyskinesia and randomization of left-right asymmetry. *Nat Genet* **30**, 143-144.

Omran, H., Kobayashi, D., Olbrich, H., Tsukahara, T., Loges, N. T., Hagiwara, H., Zhang, Q., Leblond, G., O'Toole, E., Hara, C. et al. (2008). Ktu/PF13 is required for cytoplasmic pre-assembly of axonemal dyneins. *Nature* **456**, 611-616.

Park, T. J., Mitchell, B. J., Abitua, P. B., Kintner, C. and Wallingford, J. B. (2008). Dishevelled controls apical docking and planar polarization of basal bodies in ciliated epithelial cells. *Nat Genet* **40**, 871-879.

Pennarun, G., Escudier, E., Chapelin, C., Bridoux, A.-M., Cacheux, V., Roger, G., Cl ﾃｳ ment, A., Goossens, M., Amselem, S. and Duriez, B. (1999). Loss-of-Function Mutations in a Human Gene Related to Chlamydomonas reinhardtii Dynein IC78 Result in Primary Ciliary Dyskinesia. *The American Journal of Human Genetics* **65**, 1508-1519.

Plotnikova, O. V., Pugacheva, E. N., Golemis, E. A. and Roger, D. S. (2009). Chapter 7 - Primary Cilia and the Cell Cycle. In *Methods in Cell Biology*, vol. Volume 94, pp. 137-160: Academic Press.

Quarmby, L. M. and Parker, J. D. (2005). Cilia and the cell cycle? *J. Cell Biol.* **169**, 707-710.

Rautiainen, M., Collan, Y., Nuutinen, J. and Afzelius, B. A. (1990). Ciliary orientation in the "immotile cilia" syndrome. *Eur. Arch. Otorhinolaryngol.* **247**, 100-103.

Redzic, Z. B., Preston, J. E., Duncan, J. A., Chodobski, A., Szmydynger Chodobska, J. and Gerald, P. S. (2005). The Choroid Plexus-Cerebrospinal Fluid System: From Development to Aging. In *Current Topics in Developmental Biology*, vol. Volume 71, pp. 1-52: Academic Press.

Sakai, K. and Miyazaki, J.-i. (1997). A Transgenic Mouse Line That Retains Cre Recombinase Activity in Mature Oocytes Irrespective of thecreTransgene Transmission. *Biochemical and Biophysical Research Communications* **237**, 318-324.

Salathe, M. (2007). Regulation of mammalian ciliary beating. *Annu. Rev. Physiol.* **69**, 401-422.

Satir, P. and Christensen, S. T. (2007). Overview of structure and function of mammalian cilia. *Annu. Rev. Physiol.* **69**, 377-400.

Sawamoto, K. (2006). New neurons follow the flow of cerebrospinal fluid in the adult brain. *Science* **311**, 629-632.

Shah, A. S., Ben-Shahar, Y., Moninger, T. O., Kline, J. N. and Welsh, M. J. (2009). Motile cilia of human airway epithelia are chemosensory. *Science* **325**, 1131-1134.

Thomas, J., Morlé, L., Soulavie, F., Laurençon, A., Sagnol, S. and Durand, B. (2010). Transcriptional control of genes involved in ciliogenesis: a first step in making cilia. *Biology of the Cell* **102**, 499-513.

Toskala, E., Smiley-Jewell, SM., Wong, VJ., King, D., Plopper, CG. (2005). Temporal and spatial distribution of ciliogenesis in the tracheobronchial airways of mice. *Am J Physiol Lung Cell Mol Physiol* **289**, L454–L459.

Vladar, E. K., Bayly, R. D., Sangoram, A. M., Scott, M. P. and Axelrod, J. D. (2012). Microtubules Enable the Planar Cell Polarity of Airway Cilia. *Current Biology* **22**, 2203-2212.

Wallingford, J. B. (2010). Planar cell polarity signaling, cilia and polarized ciliary beating. *Current Opinion in Cell Biology* **22**, 597-604.

Wanner, A., Salathe, M. and O'Riordan, T. G. (1996). Mucociliary clearance in the airways. *American Journal of Respiratory and Critical Care Medicine* **154**, 1868-902.

Werner, M. E., Hwang, P., Huisman, F., Taborek, P., Yu, C. C. and Mitchell, B. J. (2011). Actin and microtubules drive differential aspects of planar cell polarity in multiciliated cells. *The Journal of Cell Biology* **195**, 19-26.

Yagi, T., Tokunaga, T., Furuta, Y., Nada, S., Yoshida, M., Tsukada, T., Saga, Y., Takeda, N., Ikawa, Y. and Aizawa, S. (1993). A Novel ES Cell Line, TT2, with High Germline-Differentiating Potency. *Analytical Biochemistry* **214**, 70-76.

You, Y., Huang, T., Richer, E. J., Schmidt, J.-E. H., Zabner, J., Borok, Z. and Brody, S. L. (2004). Role of f-box factor foxj1 in differentiation of ciliated airway epithelial cells. *American Journal of Physiology - Lung Cellular and Molecular Physiology* **286**, L650-L657.

You, Y., Richer, E. J., Huang, T. and Brody, S. L. (2002). Growth and differentiation of mouse tracheal epithelial cells: selection of a proliferative population. *American Journal of Physiology - Lung Cellular and Molecular Physiology* **283**, L1315-L1321.

Yu, X., Ng, C. P., Habacher, H. and Roy, S. (2008). Foxj1 transcription factors are master regulators of the motile ciliogenic program. *Nat Genet* **40**, 1445-1453.

Acknowledgements

I am grateful to A. Kubo (Keio University) for advice on MTEC culture, and K. Sawamoto (Nagoya City University) for advice on brain ventricle IHC and M. Kiso (National Institute of Genetics) for the generation of *Ktu*$^{-/-}$ mice. I thank C. Hamilton for critical reading of the manuscript, and M. Kyokuwa for technical advice. This work was supported by Grant-in-Aid for Scientific Research on Innovative Areas from the Ministry of Education, Culture, Sports, Science and Technology of Japan.